AD-A042 320 OHIO UNIV ATHENS DEPT OF ELECTRICAL ENGINEERING F/G 1/2
INSTRUMENT LANDING SYSTEM IMPROVEMENT PROGRAM: FAR-FIELD MONITO--ETC(U)
JAN 75 DOT-FA69WA-2066

UNCLASSIFIED EER-5-21 FAA-RD-75-201 NL

| OF |
ADA
042320

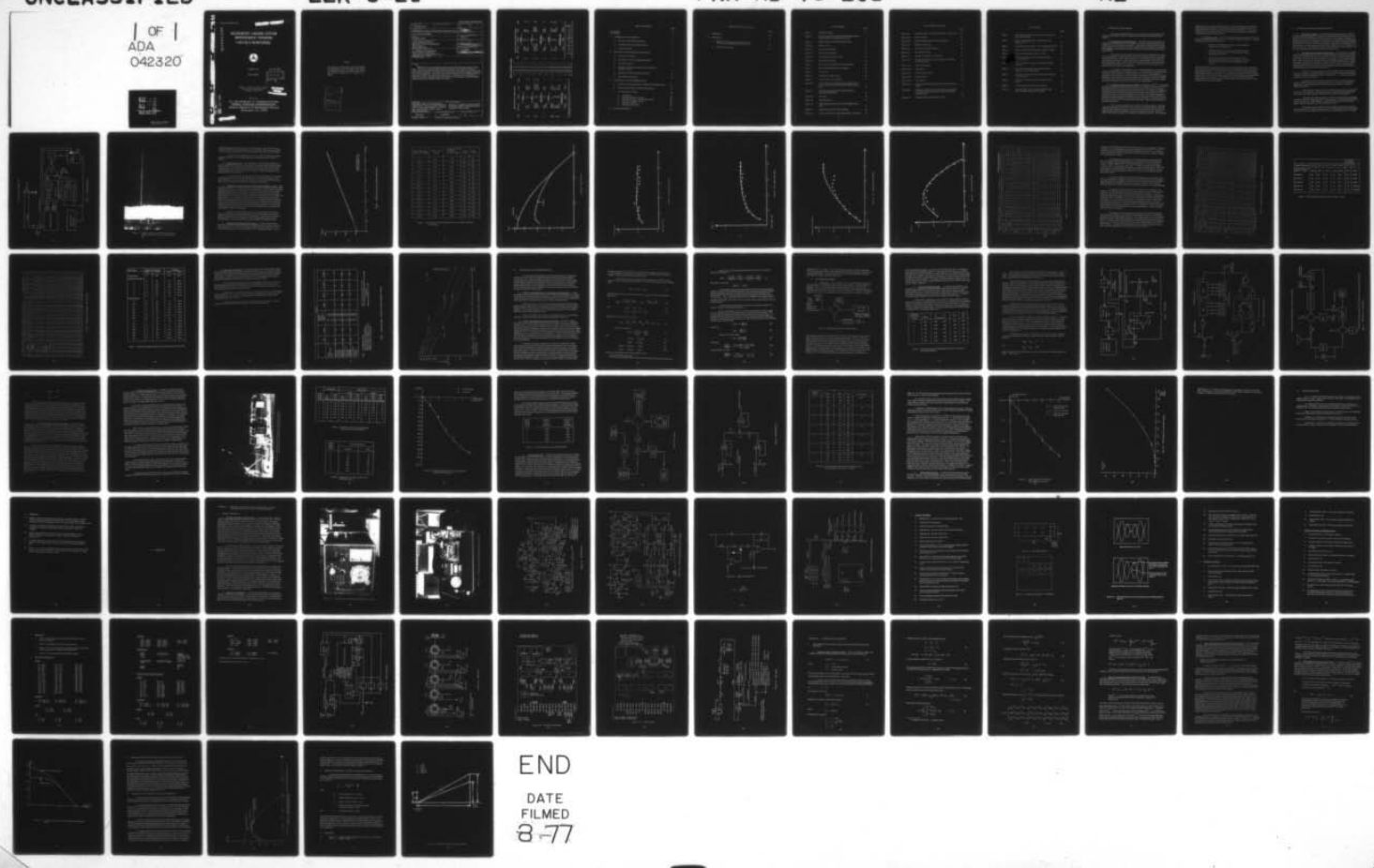

END

DATE
FILMED
8-77

Report No. FAA-RD-75-201

INSTRUMENT LANDING SYSTEM IMPROVEMENT PROGRAM: FAR-FIELD MONITORING

JANUARY 1975

FINAL REPORT

Prepared for

U.S. DEPARTMENT OF TRANSPORTATION
FEDERAL AVIATION ADMINISTRATION
Systems Research & Development Service
Washington, D.C. 20590

NOTICE

This document is disseminated under the sponsorship of the Department of Transportation in the interest of information exchange. The United States Government assumes no liability for its contents or use thereof.

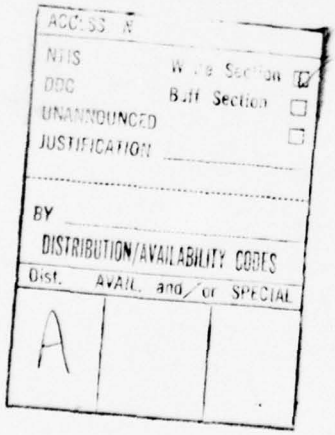

Technical Report Documentation Page

1. Report No.	2. Government Accession No.	3. Recipient's Catalog No.
FAA-RD-75-201		

4. Title and Subtitle	5. Report Date
INSTRUMENT LANDING SYSTEM IMPROVEMENT PROGRAM: FAR-FIELD MONITORING.	January 1975
	6. Performing Organization Code
	8. Performing Organization Report No. EER-5-21
7. Author(s) AVIONICS STAFF	
9. Performing Organization Name and Address Avionics Engineering Center Department of Electrical Engineering Ohio University Athens, Ohio 45701	10. Work Unit No. (TRAIS) 11. Contract or Grant No. DOT-FA69WA-2066-Mod 16
12. Sponsoring Agency Name and Address U.S. Department of Transportation Federal Aviation Administration Systems Research and Development Service Washington, D.C. 20590	13. Type of Report and Period Covered Final Report. October 1972 to January 1975. 14. Sponsoring Agency Code

15. Supplementary Notes

16. Abstract

Methods of far-field extrapolation monitoring of the ILS glide slope angle are investigated. The use of a quasilinearization algorithm to determine path angle and width from measurements below obstruction heights at the middle marker is described with results for various fault conditions tabulated. A precision space modulation quotient monitor (SMQ) for measuring high values of DDM at low signal levels is described. A description of investigations of a field strength monitor using the capture effect principle to sense changes in low altitude field strength caused by environmental effects is included.

17. Key Words	18. Distribution Statement
glide slope monitor, far field, below path measurement, difference in depth of modulation (DDM), probes, quasilinearization, extrapolation, space modulation quotient, capture effect, field strength	Document is available to the public through the National Technical Information Service, Springfield, Virginia 22161.

19. Security Classif. (of this report)	20. Security Classif. (of this page)	21. No. of Pages	22. Price
Unclassified	Unclassified	78	

Form DOT F 1700.7 (8-72) Reproduction of completed page authorized

METRIC CONVERSION FACTORS

Approximate Conversions to Metric Measures

Symbol	When You Know	Multiply by	To Find	Symbol
		LENGTH		
in	inches	*2.5	centimeters	cm
ft	feet	30	centimeters	cm
yd	yards	0.9	meters	m
mi	miles	1.6	kilometers	km
		AREA		
in^2	square inches	6.5	square centimeters	cm^2
ft^2	square feet	0.09	square meters	m^2
yd^2	square yards	0.8	square meters	m^2
mi^2	square miles	2.6	square kilometers	km^2
	acres	0.4	hectares	ha
		MASS (weight)		
oz	ounces	28	grams	g
lb	pounds	0.45	kilograms	kg
	short tons (2000 lb)	0.9	tonnes	t
		VOLUME		
tsp	teaspoons	5	milliliters	ml
Tbsp	tablespoons	15	milliliters	ml
fl oz	fluid ounces	30	milliliters	ml
c	cups	0.24	liters	l
pt	pints	0.47	liters	l
qt	quarts	0.95	liters	l
gal	gallons	3.8	liters	l
ft^3	cubic feet	0.03	cubic meters	m^3
yd^3	cubic yards	0.76	cubic meters	m^3
		TEMPERATURE (exact)		
°F	Fahrenheit temperature	5/9 (after subtracting 32)	Celsius temperature	°C

*1 in = 2.54 (exactly). For other exact conversions and more detailed tables, see NBS Misc. Publ. 286, Units of Weights and Measures, Price $2.25, SD Catalog No. C13.10:286.

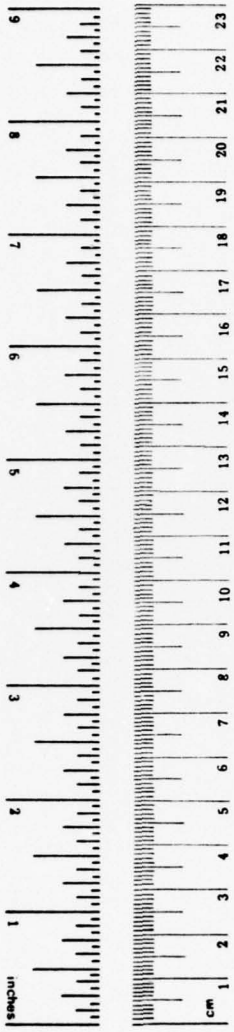

Approximate Conversions from Metric Measures

Symbol	When You Know	Multiply by	To Find	Symbol
		LENGTH		
mm	millimeters	0.04	inches	in
cm	centimeters	0.4	inches	in
m	meters	3.3	feet	ft
m	meters	1.1	yards	yd
km	kilometers	0.6	miles	mi
		AREA		
cm^2	square centimeters	0.16	square inches	in^2
m^2	square meters	1.2	square yards	yd^2
km^2	square kilometers	0.4	square miles	mi^2
ha	hectares (10,000 m^2)	2.5	acres	
		MASS (weight)		
g	grams	0.035	ounces	oz
kg	kilograms	2.2	pounds	lb
t	tonnes (1000 kg)	1.1	short tons	
		VOLUME		
ml	milliliters	0.03	fluid ounces	fl oz
l	liters	2.1	pints	pt
l	liters	1.06	quarts	qt
l	liters	0.26	gallons	gal
m^3	cubic meters	35	cubic feet	ft^3
m^3	cubic meters	1.3	cubic yards	yd^3
		TEMPERATURE (exact)		
°C	Celsius temperature	9/5 (then add 32)	Fahrenheit temperature	°F

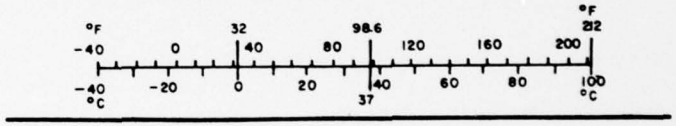

TABLE OF CONTENTS

TABLE OF CONTENTS (Continued)

LIST OF FIGURES

LIST OF FIGURES (Continued)

LIST OF TABLES

I. INTRODUCTION AND SUMMARY

This report documents the results of work performed under Modification 16 of Contract FA69WA-2066, entitled "Prototype Model Glide-Slope Gradient Clearance Monitor".

A. Philosophy of the Far-Field Monitor. The performance of a glide slope must be assured in the far field, for it is in this region that the user critically depends on the integrity of the vertical guidance information. Contemporary monitoring which involves taking samples in the near field is not always representative, and additional methods have been suggested for providing more accurate indications of the path width the user experiences in flight.

There has been a move to implement integral-type monitoring which can give a very accurate picture of path conditions provided no degrading influence exists beyond the antenna elements. Unfortunately, especially with an image-type system, there may exist disturbing influences in the environment of the antenna system. For example, the ground plane itself, which is really a part of the transmitting system may have its character changed by the addition of a cover of snow, the existence of a layer of high, wet grass, trenching or other terrain modification.

In an attempt to predict effects of environmental changes and to provide a tool to facilitate installation of new glide-slope systems, a far-field monitor is being developed. This monitor will be located at a distance greater than the $2D^2/\lambda$ measure generally accepted as a far-field criterion, and at a height not to exceed FAA obstruction clearance regulations. From an analysis of the commonality of the first Fresnel zones for the monitor and a point in the far field, it has been determined that a desirable and practical location for the far-field monitor would be in the vicinity of the middle marker.

B. Increased Scope of the Gradient Monitor. The gradient monitor[1] was originally conceived as a means for measuring the value of CDI (course deviation indicator) current of a glide path clearance structure and from this information the CDI value at 0.7 degree elevation below the nominal path angle would be predicted. This concept was implemented by developing a system of differential equations which describe the dynamics of the CDI values as a function of elevation angle above the horizontal. This system of equations is solved by a process called quasilinearization which utilizes known boundary conditions to provide the necessary parameter values for the system of equations. The equations can then be used to solve for the CDI value at the path-width angle. Appendix B gives details of this method of solution.

Given the system equations and the solution for their parameters, it becomes a straightforward matter to compute the value of CDI for any angle within the range over which the system equations are valid. During the course of this work FAA engineers suggested that the process be extended to provide also prediction of the CDI value at the nominal path angle to indicate if any changes in path angle had occurred. The information

derived from such a monitor could thus be used in setting up a glide path and minimizing initial flight check requirements. Accordingly, the scope of the gradient monitor was expanded to include prediction of both the on-path and path-width CDI. It was appropriate, therefore, to change the title of this work effort to indicate the development of a far-field glide-slope monitor (FFGSM).

C. Summary of Results. Results obtained using the data collected with the prototype far-field glide-slope monitor at the Ohio University Glide-Slope Test Site at Ravenna, Michigan, can be summarized as follows:

1. The change in path-width CDI can be closely predicted for sideband power amplitude faults.

2. Qualitative changes in the path structure during a period when there was snow-cover on the reflecting ground plane was sensed by the monitor.

3. The monitor could predict path-width values of CDI for sideband phasing faults of less than 30 degrees. For phase faults greater than 30 degrees, the predictions were not accurate.

During the analysis of the induced fault data from the Michigan Test Site, it was noted that a CDI gradient across the monitor antenna array of less than 25 microamperes would give inaccurate results. Since the height of the top antenna of the array is constrained by obstruction clearance requirements, it is not possible to sample the CDI at the greater angle required to obtain the necessary gradient for accurate predictions for sideband phase faults. However, a combination of integral-type monitoring to detect transmitting system faults, and a far-field monitor to detect changes in path structure due to environmental anomalies is believed feasible.

II. PROTOTYPE FAR-FIELD GLIDE-SLOPE MONITOR

A. Description of Location. A prototype gradient clearance monitor (GCM) was installed at the Ohio University Avionics' snow-data-collection site located at approximately 20 miles ENE of Muskegon, and 40 miles NNW of Grand Rapids, Michigan. This site was set up especially for testing of various glide-slope and related monitoring systems. The system can produce null reference, capture effect, and sideband reference glide slopes of good quality. Far-field conditions are monitored through the use of a 900-foot television tower on which probes were mounted at elevation angles of 3.0 and 2.3 degrees. The terrain at this site is relatively flat with gently rolling low hills surrounding the area. The soil in the reflecting zone consists of a fine textured black loam.

B. Description of Far-Field Glide-Slope Monitor. The FFGSM site was located approximately 4,600 feet from the Ohio University glide-slope transmitting array directly in line with the far-field television tower monitors. Initially, two dipole antenna probes were mounted on the FFGSM tower at heights of 72 and 48 feet. As the monitor evolved from a clearance monitor into a complete far-field glide-path monitor, additional probes were added. Monitoring was obtained by successive readings of CDI from the two probes which were sequentially connected to the receiver input by a coaxial switching relay. The sampled CDI values were recorded on separate channels of a Honeywell Electronik 17 strip chart recorder operating at six inches per hour.

The basic electronic equipment used for the FFGSM consists of a glide-slope receiver, meter panel, a summing amplifier, and regulated voltage supplies as described in Gradient Clearance Monitor Final Report, October, 1972 . A block diagram of the equipment used is shown in Figure 1.

A portable aluminum shelter with dimensions 9' x 6' x 6' was constructed to house the FFGSM's electronic hardware (see Figure 2). The shelter was insulated and equipped with a thermostatically controlled electric heater to maintain a relatively constant temperature.

One hundred and twenty volt, 60 Hz electrical power to the site was provided by the local utility company. The estimated line loss at normal load was approximately seven volts, and voltage regulation was employed for voltage critical equipment.

The glide-slope transmitting system at this site was continually cycled through six different modes by a sequencing switch. The modes were: three glide-path transmitting modes, (null reference, capture effect, and sideband reference) and three calibrating modes, (equality, quadrature, and 150 microamperes fly-up).

Glide-slope receiver calibration at the prototype FFGSM site was according to FAA procedure which required reference signals of 0 microamperes and 78 microamperes. Since the CDI values measured by the monitor at low elevation angles were in the range

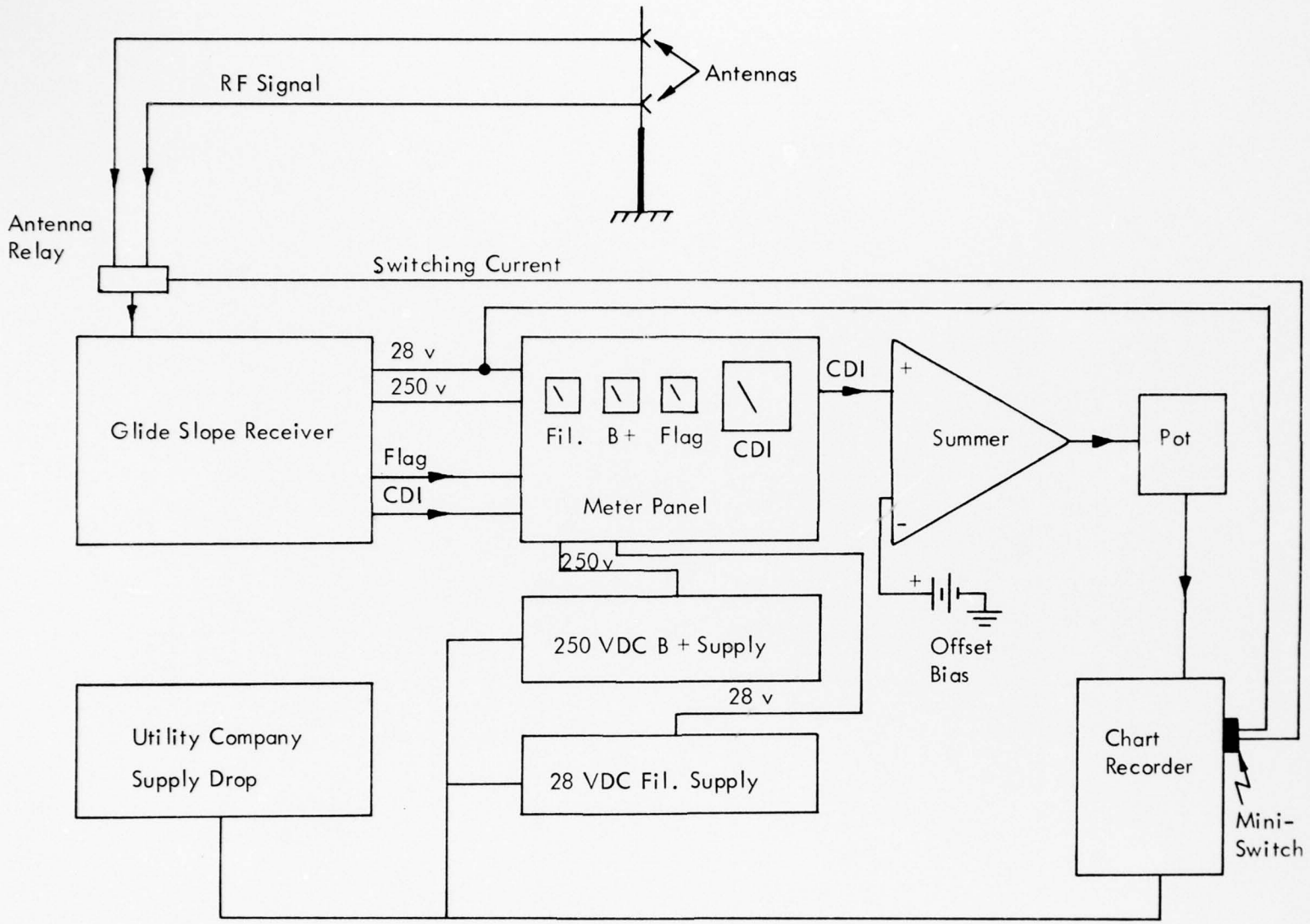

Figure 1. GCM Block Diagram.

Figure 2. Gradient Clearance Far-Field Monitoring Probes Used by Ohio University at the Michigan Snow Site.

of 300 microamperes to 400 microamperes, it was necessary to use a Scanwell Laboratories' 90/150 standard ratio generator externally to modulate a Boonton signal generator in order to produce the high values of CDI for calibration of the receiver in this range.

The ARN-18/R322 glide-slope receiver, No. 206, was calibrated using the equipment described in the preceding paragraph. The calibration curve is shown in Figure 3.

C. Plot of DDM versus α. Upon sampling the CDI at elevation angles below path at the Michigan Test Site, it was found that the values were less than those theoretically predicted. In order to obtain an accurate curve of CDI or DDM versus elevation angle (α) at this site, samples were taken at discrete intervals along the length of the vertical FFGSM tower. These data are given in Table 1, and the corresponding curves appear in Figures 4a through 4e.

It will be noted that the measured values for DDM (α) differ from the theoretical values by an increasingly greater amount for the lower angles of elevation. The shape of the DDM (α) curve corresponds to those given in the Glide Slope Manual[2] for DDM curves with a Fresnel zone reflection coefficient less than unity.

D. Installation of Additional Probes and Fault Testing of February 3, 1973. With the proposed evolution from gradient clearance monitor (GCM) to FFGSM, three additional probes were mounted on the GCM tower at the Michigan Site. The five probes were spaced uniformly between elevation angles of 0.56° and 0.87° which satisfy the 50:1 maximum obstruction height criterion. A sixth probe was also mounted at 0.94° in order to gain knowledge of conditions at higher elevation angles than are allowable under the obstruction height criterion. To investigate FFGSM credibility, an extensive series of controlled fault experiments was conducted on February 3, 1973. The measured data is presented in Table 2. The faults introduced included both phase and amplitude variations for both the null reference and sideband reference glide-slope systems. This data was analyzed using regression techniques in conjunction with a quasilinearization algorithm. The predicted values of path and width CDI, and the far-field values measured at the television tower are presented in Table 2 for comparison.

The large discrepancies between predicted CDI and measured CDI for the faults were believed to be due, at least in part, to the fact that there was very little gradient in CDI across the FFGSM receiving antenna array. Predictions at the path and width points based on monitor samples on the low-gradient portion of the CDI versus elevation angle curve, are very sensitive to small variations in the sampled values.

E. Relaxation of Obstruction Height Constraint. The far-field glide-slope monitor data of Table 1 indicates that the probe measurements were occurring on the relatively flat portion of the DDM versus elevation angle curve shown in Figure 4a. The 50:1 maximum obstruction criterion is specified for a 2.5 degree glide path. Since the

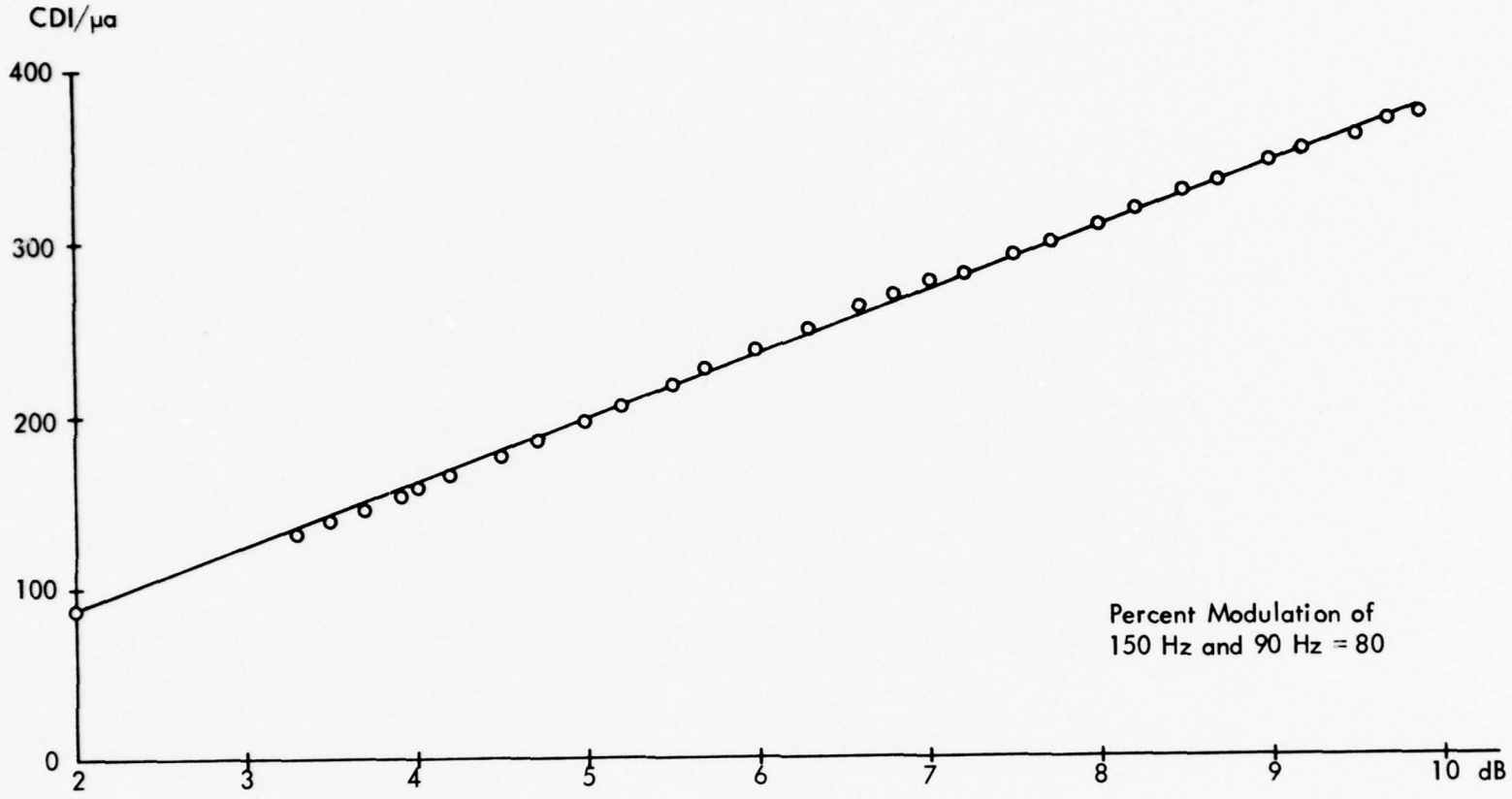

Figure 3. R322B G/S Receiver SN/206 Calibration Data.

GCM Probe Height above ground in feet	Receiver AGC in volts	Corresponding μv's of Receiver Terminal voltage	CDI in μa's	Flag in μa's
8.1	3.35	325	317	318
13.0	3.66	550	320	320
17.9	3.90	1000	320	320
22.7	4.00	1250	327	320
27.6	4.05	1350	324	320
32.5	4.11	1600	325	322
37.4	4.05	1350	326	321
42.3	4.18	1900	324	321
47.2	4.20	2000	324	321
52.0	4.25	2100	322	321
56.9	4.25	2100	320	320
61.7	4.21	2000	318	320
66.6	4.22	2000	314	320
71.5	4.31	2700	311	321
76.4	4.31	2700	306	320
81.3	4.31	2700	301	320

Table 1. Values Taken from Glide Slope Receiver as a Function of Antenna Probe Height.

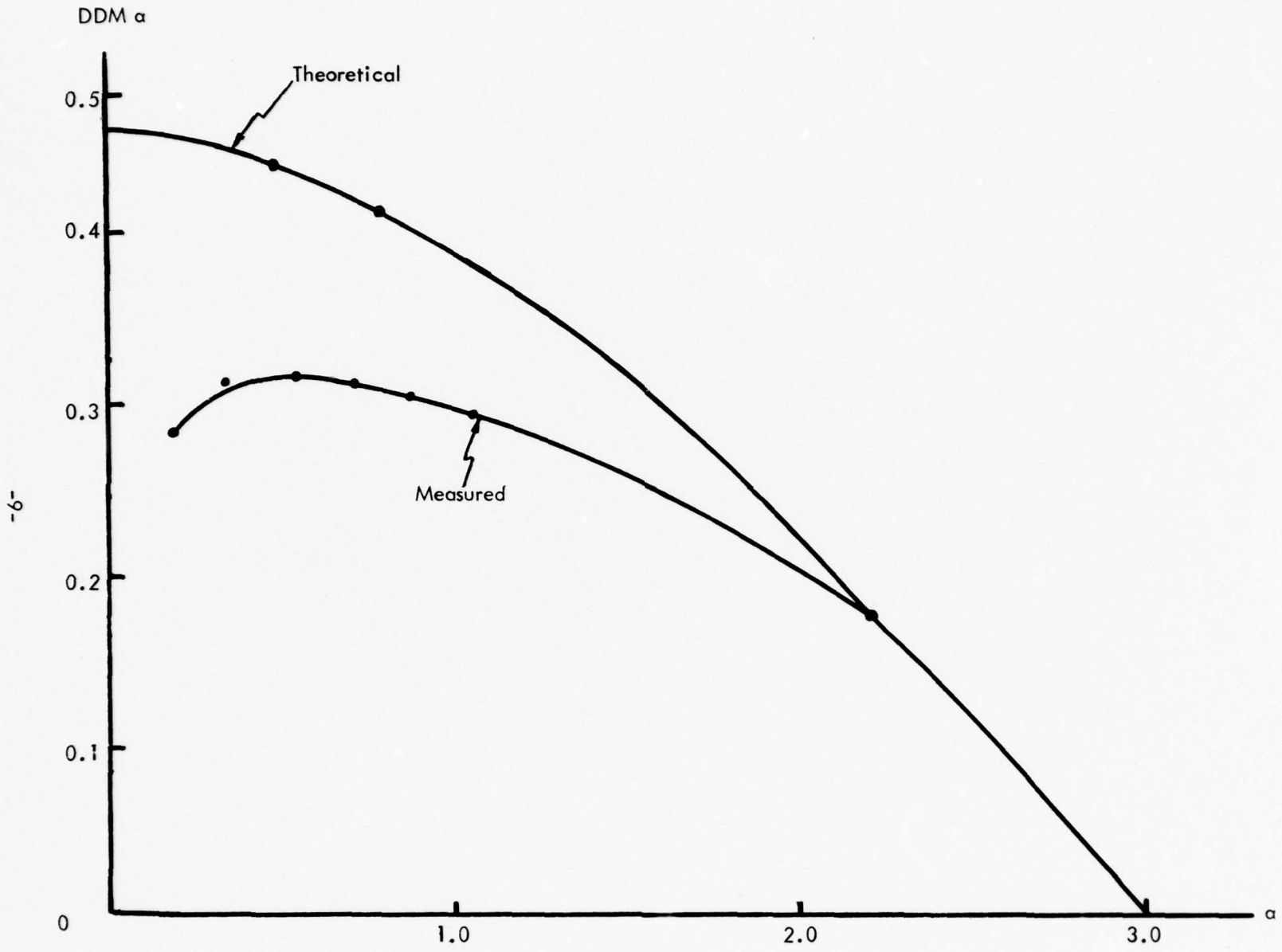

Figure 4a. DDM (α) versus α.

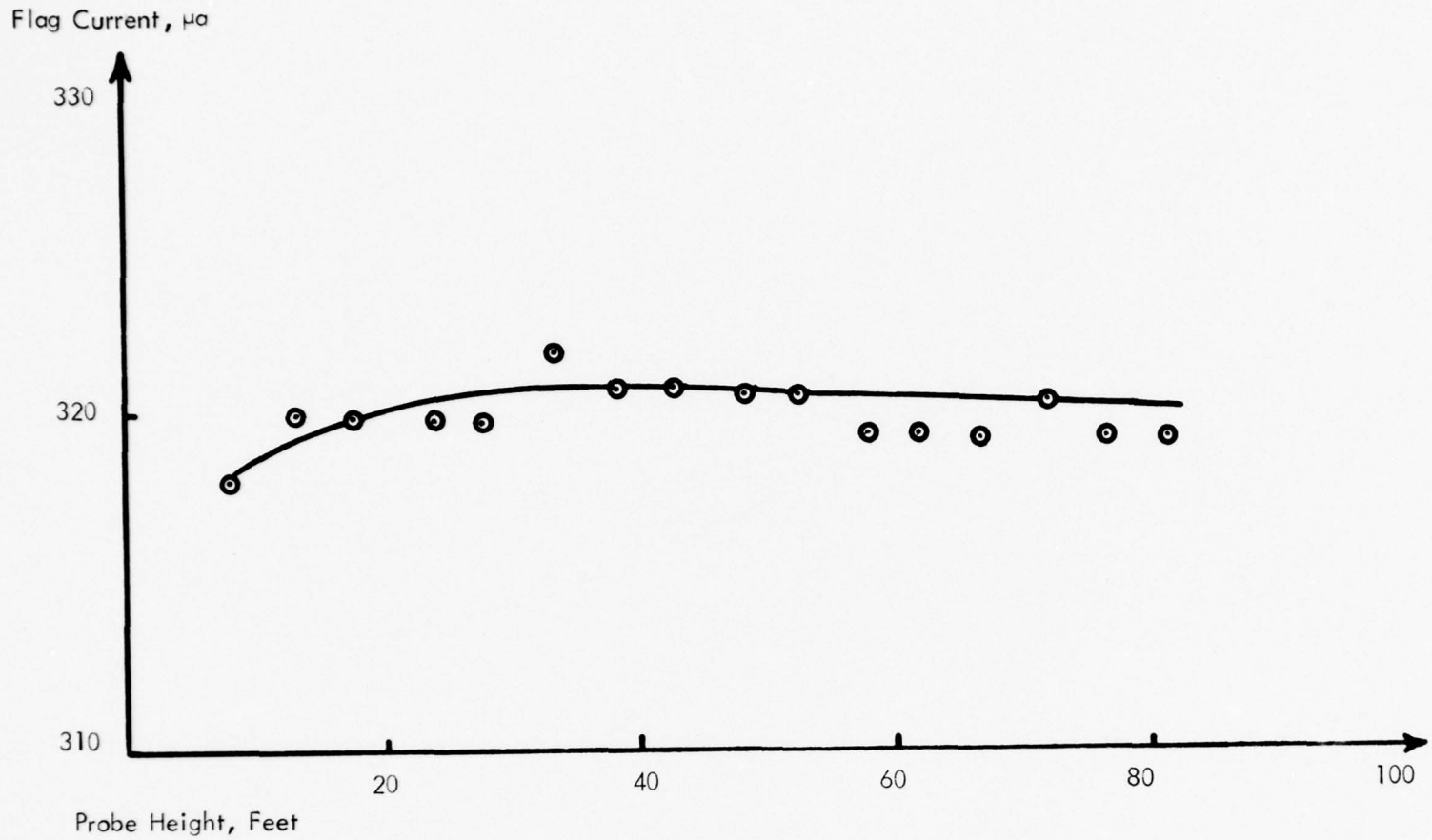

Figure 4b. Flag versus Probe Height.

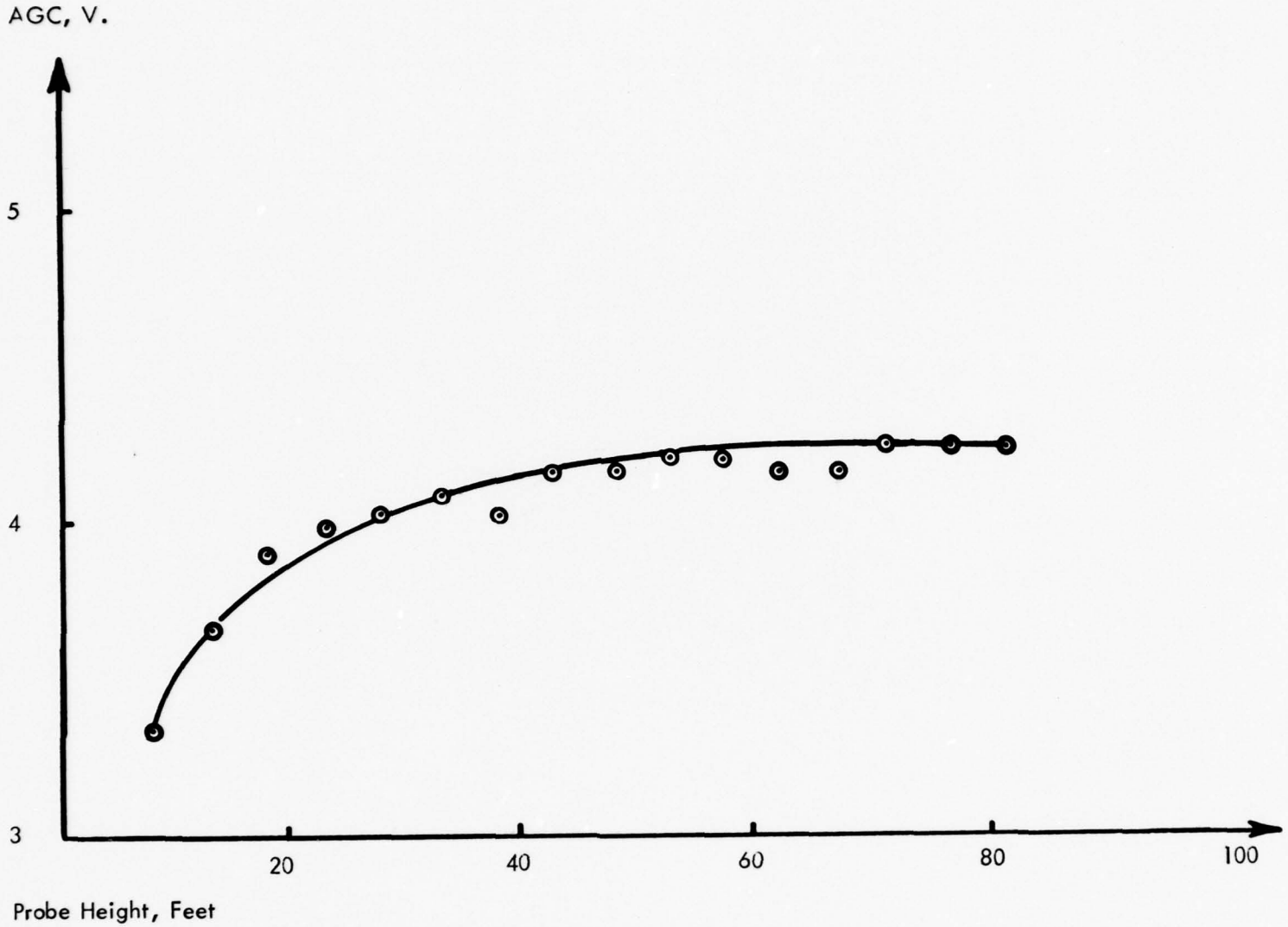

Figure 4c. AGC versus Probe Height.

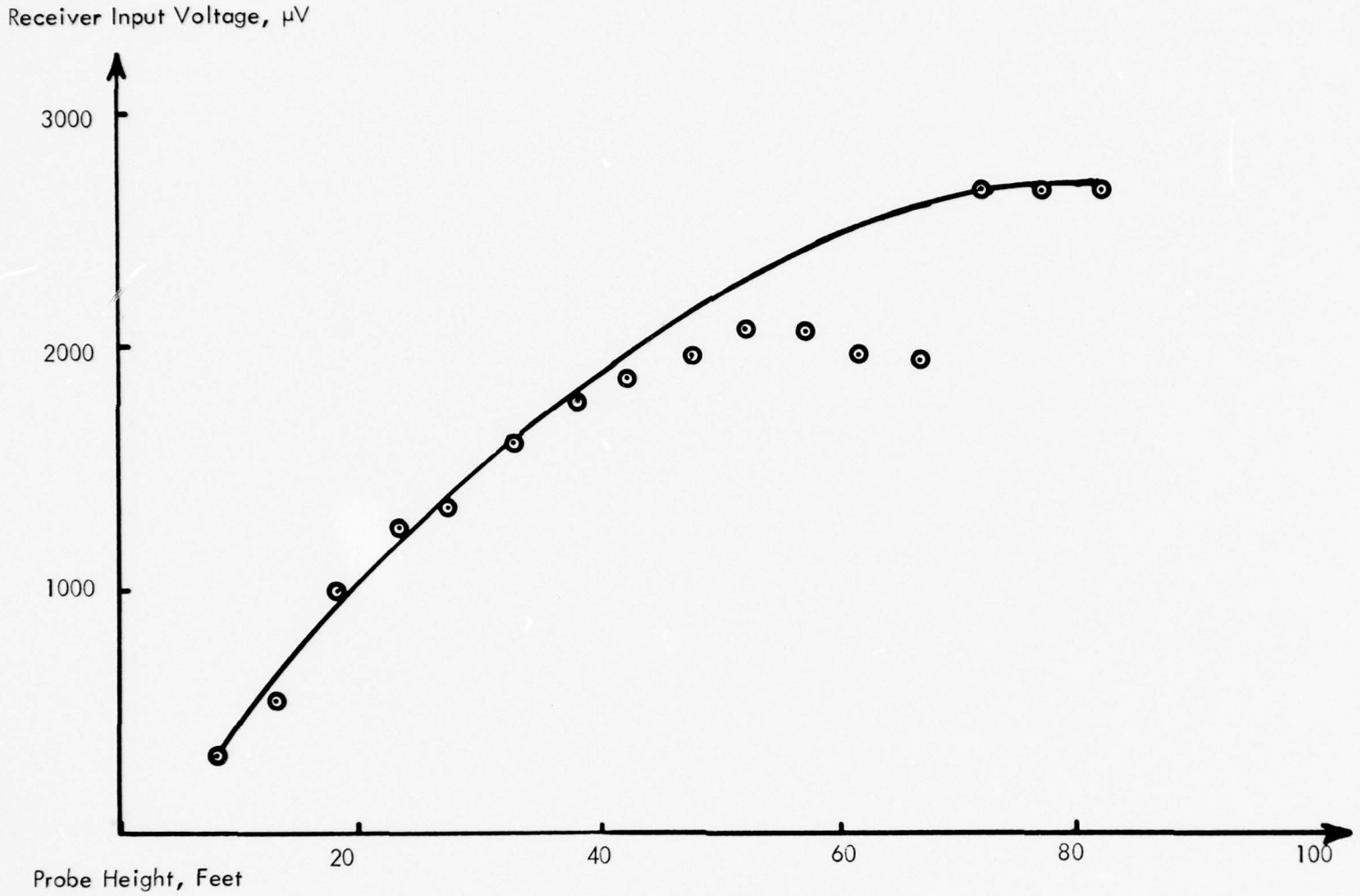

Figure 4d. Input Voltage versus Probe Height.

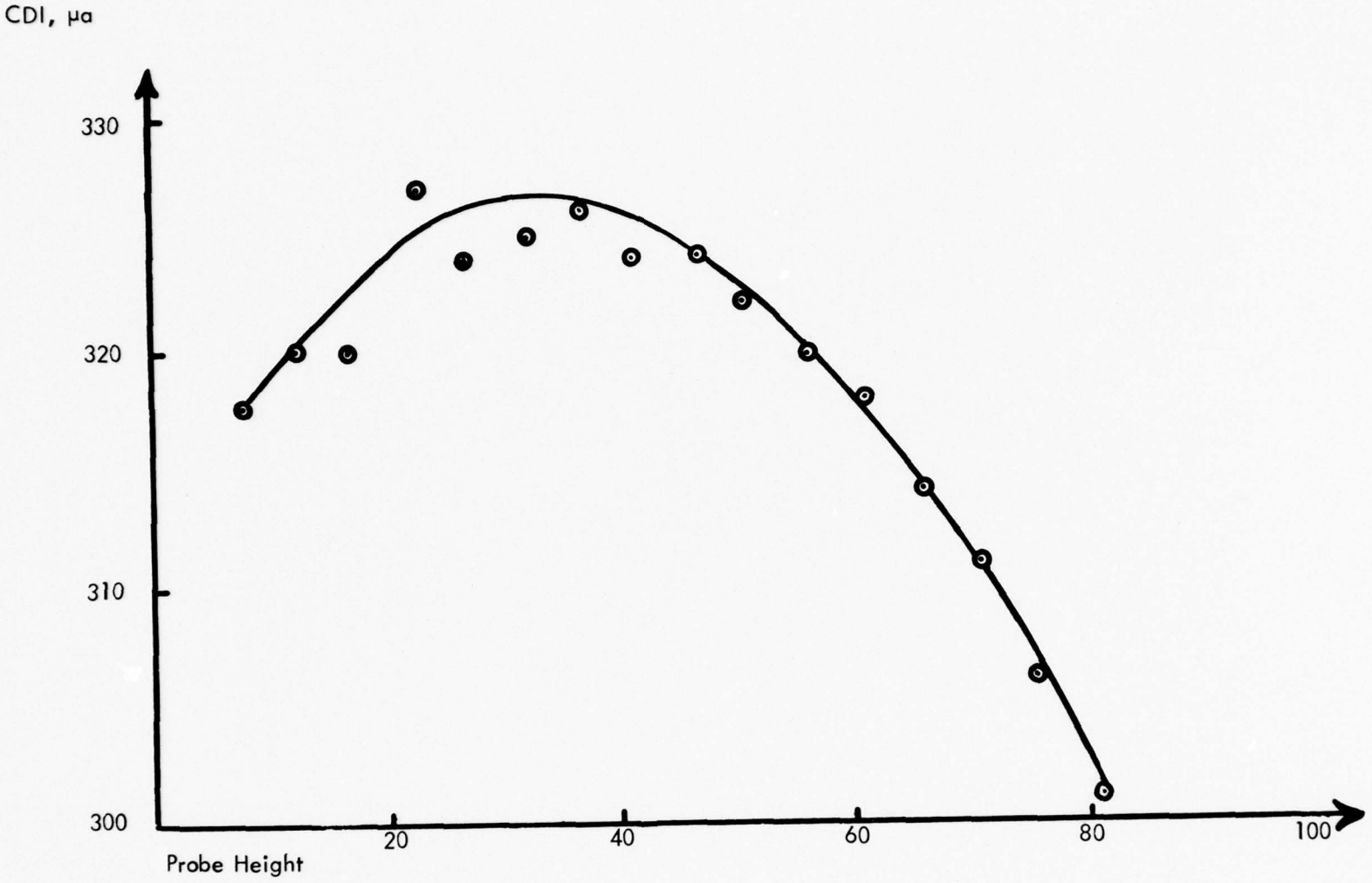

Figure 4e. CDI versus Probe Height.

20° M.P.

	X MIT	SETTING	FAR-FIELD		INTEGRAL		NEAR-FIELD		Lowest → Increasing Height GRADIENT CLEARANCE					
	Φ	A	Path	Width	Path	Width	Path	Width	1	2	3	4	5	6
CAL	Equality 32	33	0	0	0	0								-2
	Width	Cal	160	140	160	140								+145
	Quadrature		+14	+17	+4	-2								-2
NR AMP.	52	not measured	-1	+130	-2	+132	-53	+253	293	293	293	296	295	290
	52		0	+100	-1	+100	-65	+201	236	236	237	239	238	235
	52		0	+71	0	+77	-76	+151	175	175	176	176	177	175
	52		0	+152	0	+153	-38	+299	343	342	341	343	339	339 use for reference
	52		+.5	+180	0	+180	-24	>+315	379	380	380	382	381	379
	52		-2	+210	-2	+208	-15	>+315	425	425	421	423	420	416
NRΦ	52	43	0	+155	0	+151	-35	+299	337	340	340	341	343	340*
	78	43	-4	+122	+2	+129	-22	+252	288	284	283	286	289	287*
	91	43	-4	+92	-2	+100	-27	+205	226	227	229	225	228	229*
	Off Scale	43	-10	+69	-1	+71	-37	+158	170	170	173	173	175	172*
	13	43	+2	+129	-3	+122	-89	+232	269	270	270	272	270	267
	Off Scale	43	+6	+111	-3	+102	-103	+200	235	234	235	236	233	230
SR AMP.	47	43	-34	+130					394	403	406	422	425	415
	47	32	-28	+100					335	347	359	376	376	356
	47	23	-24	+75					258	272	279	296	292	276
	47	48	-34	+150					408	411	408	424	430	423
	47	57	-33	+175					411	409	402	415	425	424
	47	80	-44	+190					402	393	384	398	408	414
SRΦ	57	40	-60	+100					327	339	354	375	382	366
	67	40	-70	+79					297	310	321	350	356	338
	30	40	+19	+175					444	445	439	448	447	440
	5	40	+60	+200					450	452	445	450	439	430

*±4 μa, Average of 6 Points

Table 2. Phase/Amplitude Calibration, Michigan Snow Site, February 3, 1973.

glide path at the Michigan Test Site was 3.0 degrees, this was an unnecessarily restrictive constraint. For a 3.0 degree path, the maximum obstruction ratio is 34:1[3]. It was conjectured that raising the probes to satisfy this more liberal constraint, the probe measurements would be on the down-slope portion of the DDM (α) curve, thus providing a capability to predict more accurately.

Accordingly, the five probes of the FFGSM located at the Michigan Snow Site were raised so that the highest probe did not exceed the 34:1 maximum obstruction ratio. The angles subtended with the reflecting ground plane were now increased to 0.943°, 1.019°, 1.095°, 1.171°, and 1.247°. At these new probe elevation angles, a second series of controlled fault experiments was conducted on February 14, 1973. The data collected in these experiments is presented in Table 3. Faults introduced included both phase and amplitude variations for both the null reference and sideband reference glide-slope systems.

Results of the February 14 controlled fault experiments were analyzed using the regression predictive algorithms developed for the FFGSM. The predictions for glide-path and width CDI in microamperes and measured CDI in microamperes at the far-field probes located on the WZZM television tower are given in Table 4. The results show discrepancies between predicted values and measured values of as much as 40 microamperes.

In summary, while the accuracy of the predictions is not satisfactory, the predictions with the probe measurements at the higher angles are more consistent with the measured values than the predictions utilizing probes at the lower angles. It is to be noted, also, that several of the controlled fault perturbations are drastic enough to destroy the form of DDM (α) relationship in the far field so that prediction with this technique is not feasible. As a result of these observations, it was decided to perform another set of controlled fault experiments at the Ohio University Michigan Test Site. In this set of experiments it was especially stressed that all fault perturbations be small enough to insure that the DDM (α) theoretical far-field relationship is not disrupted. In addition, receiver calibration was to be checked frequently to prevent abnormalities in receiver characteristics from influencing the data.

The proposed set of experiments was performed for the null reference glide-slope system only on April 3, 1973, and the data is presented in Table 5. The data were processed with the FFGSM computer algorithm. The predicted CDI values at the path and width points along with the values measured at the far-field television tower are given in Table 6. It will be noted that the predictions for sideband amplitude faults are reasonably consistent with the far-field values. This is also true for sideband phase faults of up to about 30 degrees. However, for sideband phase faults in excess of 30 degrees, the predictions are not consistent with the values measured in the far field.

	X MIT	SETTING	FAR-FIELD		INTEGRAL		NEAR-FIELD		GRADIENT CLEARANCE					
	Φ	A	Path	Width	Path	Width	Path	Width	1 (Top)	2	3	4	5	6 (Bot.)
CAL	52 Equality	33	+1	0	0	0			-1					
	Width	Cal	+165	+155	+165	+155			+166					
	Quadrature		+17	+15	0	+2			-26					
NR AMP.	52	not measured	+3	+130	0	+127	-58	+235	+276	+291	+293	+308	+314	+317
	52		0	+100	-1	+98	-70	+189	+230	+241	+241	+254	+260	+258
	52		-1	+71	-2	+69	-84	+142	+166	+177	+179	+188	+194	+196
	52		+2	+152	+2	+145	-46	+280	+329	+343	+343	+358	+365	+364
	52		+3	+180	0	+169	-31	>+320	+372	+390	+400	+408	+416	+419
	52		+1	+195	-2	+187	-26	>+320	+399	+414	+425	+431	+431	+435
NRΦ	52	+43	+4	+138	-1	+120	-67	+245	+286	+303	+312	+320	+328	+332
	78	+43	-6	+115	-1	+105	-34	+237	+274	+288	+293	+297	+304	+301
	91	+43	-10	+95	-2	+90	-29	+206	+234	+250	+254	+258	+264	+262
	Off Scale	+43	-12	+69	-2	+67	-31	+166	+186	+200	+199	+201	+205	+204
	13	+43	+10	+105	-2	+90	-124	+163	+187	+194	+204	+214	+220	+223
	30	+43	+8	+130	-2	+115	-98	+213	+256	+264	+274	+282	+290	+292
SR AMP.	47	+43	-18	+130					+412	+423	+435	+438	+445	+454
	47	+32	-10	+100					+331	+345	+356	+362	+373	+386
	47	+19	-5	+75					+200	+209	+217	+220	+231	+242*
	47	+46	-16	+150					+372	+391	+396	+405	+413	+422*
	47	+53	-16	+175					+379	+397	+407	+415	+421	+433*
	47	+76	-24	+190					+408	+417	+429	+435	+441	+450*
SRΦ	57	+40	-43	+121					+308	+319	+337	+337	+348	+358
	67	+40	-61	+110					+295	+306	+317	+321	+335	+342
	30	+40	+9	+180					+420	+425	+429	+435	+440	+442*
	5	+40	+51	+212					+425	+431	+437	+440	+423	+451*

*Average of Six Readings ± 4-8 μa

Table 3. Controlled Faults Experiments, No. 2, February 14, 1973.

						Algorithm Predictions	
Angles of Elevation	0.60°	0.66°	0.72°	0.78°	0.84°	2.3°	3.0°
Nominal data for 3° path, 0.7° width	386μa	382μa	377μa	372μa	367μa	143	4/90Hz
1st data set	386	387	372	377	367	145	1/90Hz
2nd data set	381	387	372	377	362	143	3/90Hz
3rd data set	396	372	397	362	377	145	4/90Hz
4th data set	386	402	377	372	367	68	112/90Hz
5th data set	386	382	377	352	367	59	119/90Hz

Table 4. Monitor Data and Predicted Values, February 14, 1973.

X MIT	SETTING	FAR-FIELD		INTEGRAL		NEAR-FIELD		GRADIENT CLEARANCE					
		Path	Width	Path	Width	Path	Width	1	2	3	4	5	6
Equality		0	-1	-1	-2	-117	+15	+3					
Width	Cal	+156	+148	+165	+159	+109	+242	+175					
Quadrature		+12	+9	0	+3	-168	+3	-45					
(Nominal) 127	0	+1	+149	0	+140	-76	+258	303	309	318	323	325	327
130	0	+1	+140	-1	+134	-78	+244	287	293	302	306	308	310
134	0	0	+130	-2	+124	-82	+228	270	276	284	288	291	292
140	0	0	+120	-2	+118	-86	+209	249	253	261	266	268	270
84	0	0	+160	0	+150	-70	+280	325	331	340	346	347	350
Had to change X MIT SBA	0	+1	+170	-1	+162	-64	+298	343	350	360	365	366	368
		+2	+180	0	+173	-62	+310	356	364	372	378	379	381
(Nominal) 127	0	0	+150	-1	+144	-74	+263	306	313	322	328	329	330
127	-5°	+1	+150	-1	+140	-79	+258	301	307	317	322	325	327
127	-10°	+2	+150	-1	+144	-82	+255	296	302	312	318	320	323
127	-15°	+3	+150	-1	+140	-86	+252	292	299	309	315	318	319
127	-30°	+6	+143	-1	+135	-96	+235	269	274	285	291	294	297
127	-40°	+7	+135	-1	+130	-108	+217	244	248	260	267	271	273
127	-50°	+9	+124	-1	+119	-117	+195	214	217	228	235	240	242
127	-60°	+10	+109	-1	+103	-127	+168	175	178	189	196	201	203
127	+5°	0	+150	-2	+142	-72	+264	308	315	323	328	330	331
127	+10°	0	+148	-2	+142	-70	+262	308	314	323	329	331	332
127	+15°	-1	+146	-1	+140	-68	+262	308	315	322	327	328	330
127	+30°	-4	+135	-2	+130	-60	+253	300	307	313	316	316	317
127	+40°	-6	+124	-2	+121	-55	+239	286	292	296	299	299	299
127	+50°	-7	+110	-2	+110	-53	+218	264	271	273	274	273	274
127	+60°	-9	+90	-2	+91	-51	+189	233	239	240	240	238	238

Table 5. Michigan Snow Site Data, April 3-4, 1973.

Fault Types	Measured (Far Field)		Predicted	
	Path	Width	Path	Width
Nominal Path	+1	149	+2.7	146.5
Sideband Amplitude:				
1	+1	140	+2.6	138.9
2	0	130	+1.2	130.0
3	0	120	+0.5	119.3
4	0	160	+4.7	157.9
5	+1	170	+5.6	167.2
6	+2	180	+7.6	174.4
Sideband Phase:				
-5°	+1	150	-0.2	144.2
-10°	+2	150	-1.3	141.3
-15°	+3	150	-3.9	138.2
-30°	+6	143	-6.0	125.9
-40°	+7	135	-12.2	110.8
-50°	+9	124	-14.0	95.3
-60°	+10	109	-18.7	74.4
+5°	0	150	+3.8	149.6
+10°	0	148	+1.7	148.4
+15°	-1	146	+6.5	150.9
+30°	-4	135	+11.5	149.6
+40°	-6	124	+14.1	143.9
+50°	-7	110	+18.0	135.5
+60°	-9	90	+19.8	121.5

Table 6. Predicted and Measured CDI Values for Fault Tests of April 3, 1973.

F. Scale Model Measurements. Scale model measurements of DDM gradient response and far-field DDM response to coverages of polystyrene dielectric on a near-perfectly conducting ground were considered desirable because of the greater flexibility that could be obtained using models. Fortunately, the Air Navigation Group at the University of Sydney, Australia, were involved in scale measurements of glide-slope systems. They responded favorably to a request for measurements of the gradient and these are presented in Table 7.

The perturbation of the environment was accomplished by placing 1/10 inch thick sheets of polystyrene for effectively 3000 feet on the flat conducting ground plane. At a 30:1 scale factor, this amounted to an equivalent 3-inch thickness of, say, ice which could have a similar relative dielectric constant of 2.56.

Unfortunately, the resulting data is in many respects inconsistent with data obtained from full scale work. No reason can be given for these inconsistencies; however, there is sufficient confidence in the numbers to encourage further investigation of the model and its representativeness of the real world.

A sample of data analysis assuming a cosine law is shown in Figure 5. This best describes the relationship between the gradient observation and the far field.

	RANGE						
	921'	3040'	Gradient Monitor Probe Site 4000'	6080'	9120'	12,160'	15,200'
Ideal 3° Unperturbed Site	2	2	1.15° -335 .9 -362 .75 -374 .60 -380	0	-2	2	-2
Site with 3° 1/10 Inch Dielectric Covering	10	16	1.15 -296 .9 -320 .75 -334 .60 -340	11	8	12	5
Site with 3° 2 x 1/10 Inch Dielectric Coverage	-190	-118	1.15 -390 .9 -404 .75 -419 .60 -425	-103	-100	-93	-100
Site with 3° 3 x 1/10 Inch Dielectric Coverage	-85	-65	1.15 -356 .91 -386 .75 -400 .60 -408	-57	-60	-50	-60

Note: Null Reference System
Values are given in microamperes
Positive Values = 90 Hertz, Fly Down
Negative Values = 150 Hertz, Fly Up
Distances are from the glide slope

Path width 150 μa to 150 μa = 1.44°
Antenna masts on runway centerline with no offset of antennas
Polystyrene Dielectric $E_n = 2.56$

Table 7. Scale Model Data. Courtesy of University of Sydney, Australia.

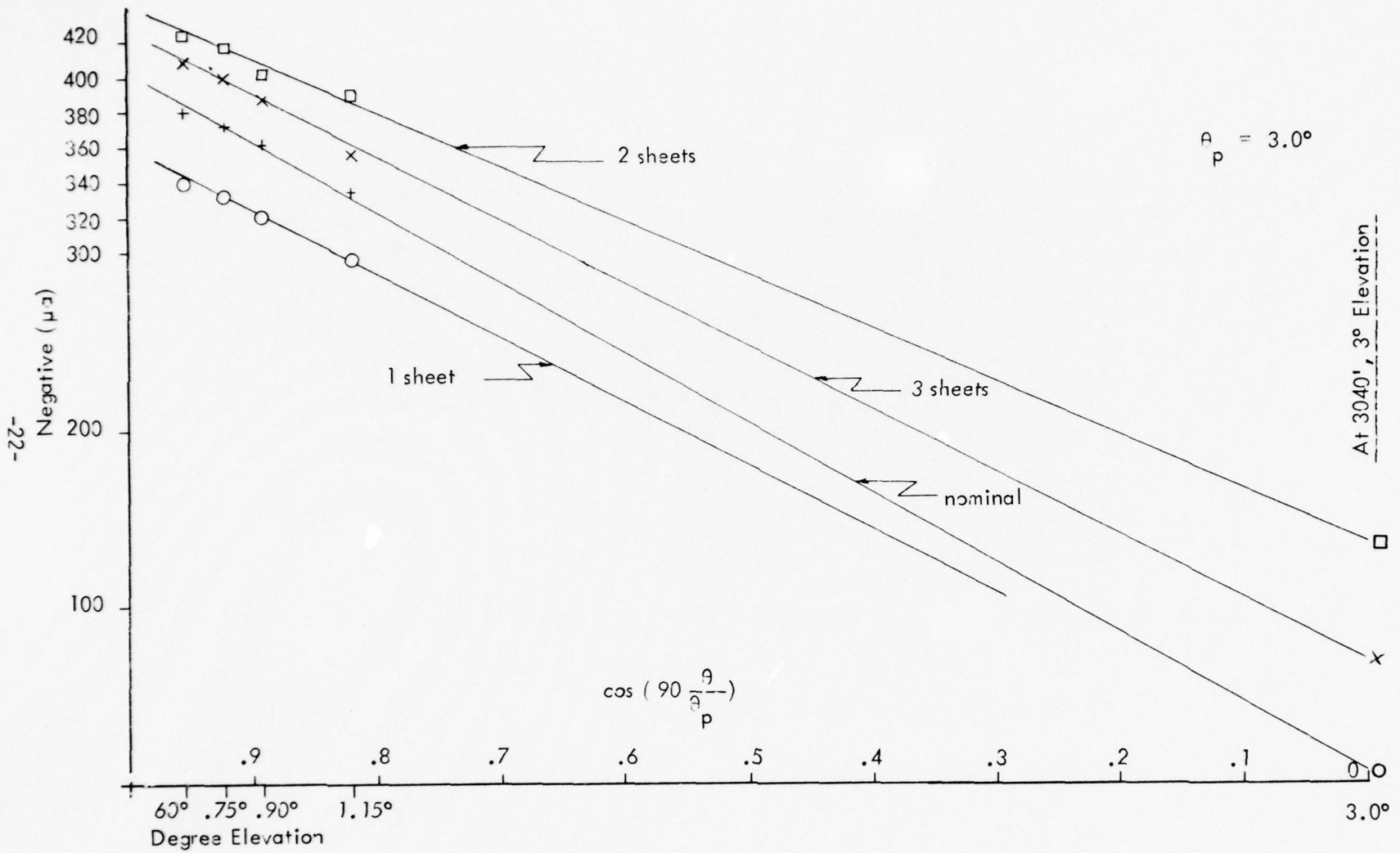

Figure 5. Plot to Examine Curve Fitting for Measured Data.

III. CONCLUSIONS AND RECOMMENDATIONS

An examination of the foregoing data and predictions based on extrapolation indicate that a more careful study of the basic phenomena and of the instrumentation involved is in order. Factors not taken into account in the calculations but which may be responsible for the apparent anomalous behavior of the CDI at very low angles include (a) the antenna patterns of the probes used in making the measurements, (b) interaction between adjacent probes, (c) the nonlinearity of the AGC action for weaker signals, (d) the variation of the reflection coefficient with angle of incidence, and (e) the effects of noise on the difference measurements.

A. Artificial Ground Plane Faulting - Conductive Comb Experiments. In order to implement a more basic evaluation of the problem of below-path measurements, a method of producing strictly environmental disturbances in the path has been devised. This consists of placing triangular metallic screens in the first Fresnel zone to change the reflected signal (image portion of the space distribution) without changing the direct signal.

Preliminary test runs at the Ohio University Tamiami test site with three equilateral triangular screens 8 feet on a side placed across the first Fresnel zone show varying degrees of effect on the position of the glide slope depending on whether they are placed ahead of, at, or beyond the specular point. Further experimentation with more screens is indicated in order to obtain definitive results.

Further scale model measurements are recommended to obtain more conclusive information on glide-slope effects due to dielectric ground-plane coverings.

B. Precision Space Modulation Quotient Measurement. To obviate problems arising from the use of glide-slope receivers beyond their design CDI range, an adaptation has been made of an Ohio University designed precision localizer audio to DC converter. This device accepts the audio from a standard localizer receiver such as the Narco NAV-11, filters it through specially designed narrow band active filters, converts it to two DC voltages proportional to the 90 and 150 Hz audio respectively and then divides the difference of these voltages by their sum. This quotient will be proportional to CDI, the proportionality constant depending upon the modulation index of the transmitter, m, and the ratio of E_{ss} to E_{cs}, A. Since any change in these factors will be detected by the integral monitor, the quotient, which will be referred to as the Space Modulation Quotient (SMQ), will serve to study the environmental effects.

A standard ILS receiver will produce a CDI which is proportional to DDM, only if the automatic gain control (AGC) is capable of maintaining a constant IF signal level at the second detector over the dynamic operating range of interest. Since the RF signal levels are low at the low angles encountered in below-path monitoring, the AGC may not be adequate, which will cause the CDI to become a function of RF signal strength. The audio processor developed at Ohio utilizes an analog divider to divide the voltage proportional to the difference in depth modulation (DDM) by a voltage proportional to the sum of depths of modulation (SDM). In this way, if a change is applied, RF signal allows the sum of the 90/150 Hz composite of the second detector to change, the analog divider

cancels out this change in the output. Any change in the composite due to a change in m is also canceled. The output of this processor then is proportional to SMQ which will be shown in the following derivation to equal DDM/m.

Using the notation of FAA Manual FV-106-1 of February, 1971[4], and FAA Manual FV-301, the relationships among DDM, CDI, and SMQ are easily derived. Starting with:

$$DDM = M_{150} - M_{90} \tag{1}$$

(since the interest here is in below-path monitoring, M_{150} will always be greater than M_{90}) where:

$$M_{150} = \frac{E_{cs150} + E_{ss150}}{E_c} \qquad M_{90} = \frac{E_{cs90} - E_{ss90}}{E_c} \tag{2}$$

and:

$$E_{cs150} = E_{cs90} = mE_c \tag{3}$$

$$E_{ss150} = E_{ss90} = sE_c = mAE_c \tag{4}$$

substituting (2), (3), and (4) into (1) gives:

$$DDM = \frac{mE_c + mAE_c}{E_c} - \frac{mE_c - mAE_c}{E_c} = 2mA = 2s \tag{5}$$

SMQ is, by definition:

$$SMQ = \frac{E_{dc150} - E_{dc90}}{E_{dc150} + E_{dc90}} \tag{6}$$

but:

$$E_{dc150} = K_r E_{ac150} \tag{7}$$

$$E_{dc90} = K_r E_{ac90} \tag{8}$$

$$E_{ac150} = K_d(E_{cs150} + E_{ss150}) \tag{9}$$

$$E_{ac90} = K_d(E_{cs90} - E_{ss90}) \tag{10}$$

where E_{dc} is the rectified output of the magnitude circuit.

E_{ac} is the detected audio output.

K_r and K_d are the proportionality constants of the rectifier and demodulator respectively.

Again using (3) and (4) and substituting (9) and (10) into (7) and (8) and thence into (6) results in:

$$SMQ = \frac{K_r K_d(mE_c + mAE_c) - K_r K_d(mE_c - mAE_c)}{K_r K_d(mE_c + mAE_c) + K_r K_d(mE_c - mAE_c)} = 2A$$

from which it is seen that:

$$m(SMQ) = (DDM)$$

In ordinary glide-slope and localizer receivers the CDI is made proportional to DDM by the use of AGC which (theoretically) holds the response independent of signal strength and therefore obviates the necessity of dividing the audio difference by the carrier strength, when the meter has been calibrated to respond with the proper CDI for a known $M_{150} - M_{90}$. For greater precision the use of SMQ frees the measurement from the effects of variation of the AGC action at its extreme ranges as encountered at very low monitoring angles.

The SMQ Monitor supplied under this contract is described in detail in the instruction manual included here as Appendix A.

Further investigation of the low angle far-field monitoring problem suggests that still another quantity, the Audio Frequency Clearance (AFC) may be useful. This ratio can easily be determined by making a slight modification of the SMQ Meter. It is the ratio of the DC recovered from the 150 Hz audio to that from the 90 Hz modulation. Ideally this is proportional to the radio frequency clearance (RFC) described in FAA Manual FV-301, where it is shown that:

$$DDM = 2m\frac{RFC - 1}{RFC + 1} \tag{11}$$

from which

$$SMQ = 2\frac{RFC - 1}{RFC + 1} \tag{12}$$

Solving (11) for RFC yields:

$$RFC = \frac{2m + DDM}{2m - DDM} \tag{13}$$

from which

$$\frac{d(RFC)}{d(DDM)} = \frac{(2m - DDM) + (2m + DDM)}{(2m - DDM)^2} \tag{14}$$

and since $DDM \approx 2s \approx 2mA$

$$\frac{d(RFC)}{d(DDM)} = \frac{4m}{(2m - 2Am)^2} = \frac{1}{m(1 - A)^2} \tag{15}$$

Substitution of m = 0.4 and A = 0.3 into (15) gives a value of 5.1 for the derivative. Thus, for these typical values the RFC (and therefore the AFC) is changing over five times as rapidly as the DDM. It is concluded that further studies might benefit by using this more rapidly changing measure for extrapolation.

C. Low Angle Capture Monitor.

1. Introduction. In an attempt to develop a far-field glide-slope monitor that could sample the below-path signal and predict from changes in the signal what was happening on path, a monitoring scheme was proposed by H. H. Butts, an FAA engineer, that was based on the principle that the stronger of two RF signals within the band pass of the receiver has the ability to capture the receiver.[5] Figure 6 is a simplified diagram of the system. The predominantly 150 Hz modulated received signal is combined

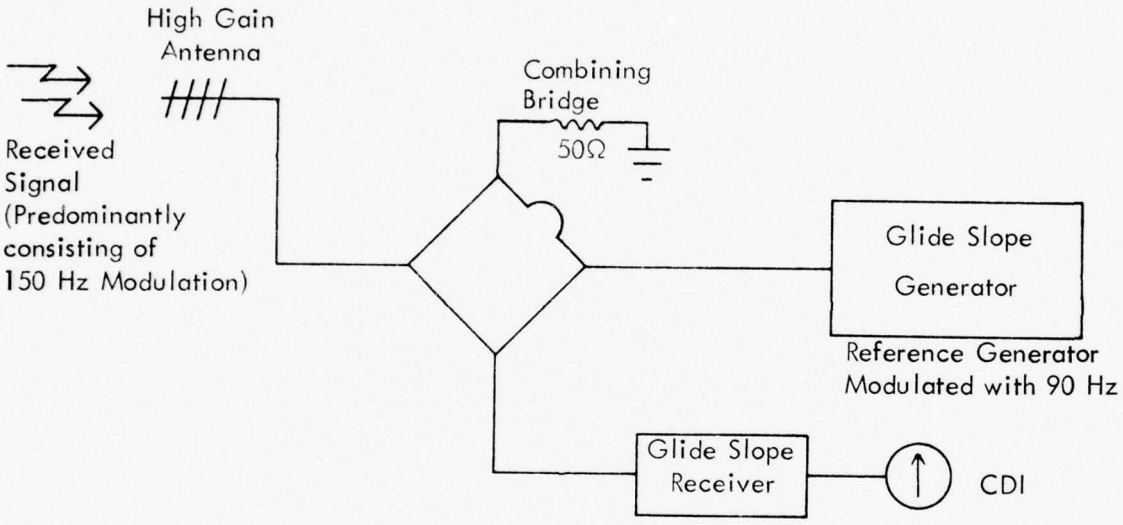

Figure 6. Block Diagram of Capture Monitor System.

with a reference signal that is modulated by 90 Hz audio. The frequency of the reference signal is offset from that of the received signal by approximately 10 KHz. The two signals are combined and fed to a typical glide-slope receiver. If the signal level of the received signal is much greater than that from the reference generator, the CDI output will read a high positive level indicating a predominance of 150 Hz audio information. (A positive CDI reading corresponds to a fly-up, or 150 Hz signal, while a negative CDI reading corresponds to a fly-down, or 90 Hz signal.) As the signal level of the received signal decreases, the CDI output will go toward zero until the received signal level drops below that from the reference generator, with the CDI output now increasing in the negative sense. The rationale behind using this capture principle is that changes in the

reflecting ground plane height, as caused by the accumulation of snow, will change the lobe structure of the glide-path signals. At low angles, this will show up as a change in the amplitude of the received signal which, when combined with a stable reference signal, will show up as a change in the receiver's CDI output. It is hoped that this monitor scheme will help to eliminate to a great degree all of the problem areas encountered with the far-field gradient clearance monitor. By properly setting the reference generator level, the receiver audio circuitry will be operating around the zero CDI level, where the most linear receiver response is obtained.

2. Theory and Preliminary Design. As stated in the introduction, the idea behind the below-path far-field glide-slope capture monitor (GSCM) is to monitor signal strength to detect environmental changes, specifically changing ground-plane levels due to snow cover. The received signal is combined with a reference signal, and the reference generator signal level is set to give a CDI reading near zero. A change in the received signal strength will then show up as a change in the CDI output.

If the ground is considered as a flat, perfectly-conducting plane of infinite extent and snow cover is considered simply as only a rise in the height of the ground plane, then for a null reference glide-slope system, this rise in the ground plane will result in a decrease in signal level at the monitor. Table 8 gives some ideal, calculated parameter values as received at the middle marker by a monitor probe mounted 30 feet above ground in the field of a 3° nominal glide-slope signal.

Change in Ground Plane (Feet)	α Degrees	E_{ss} (Normalized)	E_{cs} (Normalized)	DDM	CDI μa
0	.382	.3887	.1983	.470	403
1	.369	.3638	.1784	.489	419
2	.357	.3394	.1594	.511	439
3	.344	.3157	.1411	.537	460
4	.331	.2927	.1237	.568	486
5	.318	.2705	.1073	.605	518

Table 8. Calculated Field Strength DDM and CDI Values for Changes in Ground-Plane Height.

As can be seen, a shift in ground plane height of 5 feet decreases the value of E_{ss} to .7 times its normal value, and decreases the value of E_{cs} to .54 times its normal value. It is hoped that this decrease in the combined received signal strength will show up in a magnified form at the CDI output of the receiver.

To utilize the capture effect, the reference generator must be offset from the frequency of the received signal by a small amount that is still within the passband of the receiver. Using two, 20-channel, crystal-controlled Boonton Type 232-A glide-slope test generators, one simulating the received signal, and the other as the reference generator, the frequency difference was measured for the 20 channels. The frequency difference for the 20 channels ranged from 300 to 23,000 Hertz, which was within the advertised limits of the crystal accuracy. It was also found that, with 150 Hz only modulation on one generator and 90 Hz only modulation on the second generator, the output of the receiver indicated a zero CDI value when the signal levels of the two generators were approximately equal, provided the frequency difference of the two generators was greater than 2,000 Hz. For values less than 2,000 Hz, the CDI output became very erratic.

A prototype of the GSCM as assembled and bench tested is shown in Figure 7. For bench testing, a second signal generator replaces the Yagi antenna. The output of the reference generator is fed to a HP 10514 Balanced Mixer. The RF output of the mixer is then measured by a vector voltmeter and the output of the VVM is used with appropriate circuitry to provide AGC action to eliminate unwanted amplitude variations in the RF output from the reference generator. Figure 8 illustrates this AGC arrangement.

A circuit to monitor the difference frequency is shown in Figure 9. The output from the reference generator is combined with an amplified received signal in a second bridge, then detected to get the difference frequency (see Figure 7), and the detected IF fed to the frequency counter circuit. The output of the counter circuit presently is recorded on a chart recorder, but can be used to provide frequency control if necessary to insure a proper frequency difference between the two signals. This automatic frequency control is helpful both during initial monitor setup and also during monitor operations if a transmitter change occurs.

One problem that arose was that of phase variation of the 90 Hertz component of the received signal and the 90 Hertz modulation of the reference signal. From the equation:

$$M_{150} + M_{90} = 2m = .8$$

and

$$M_{150} - M_{90} = DDM$$

and the fact that for a 3° glide slope, at an altitude of 30 feet at the middle marker, the DDM = .470, one gets:

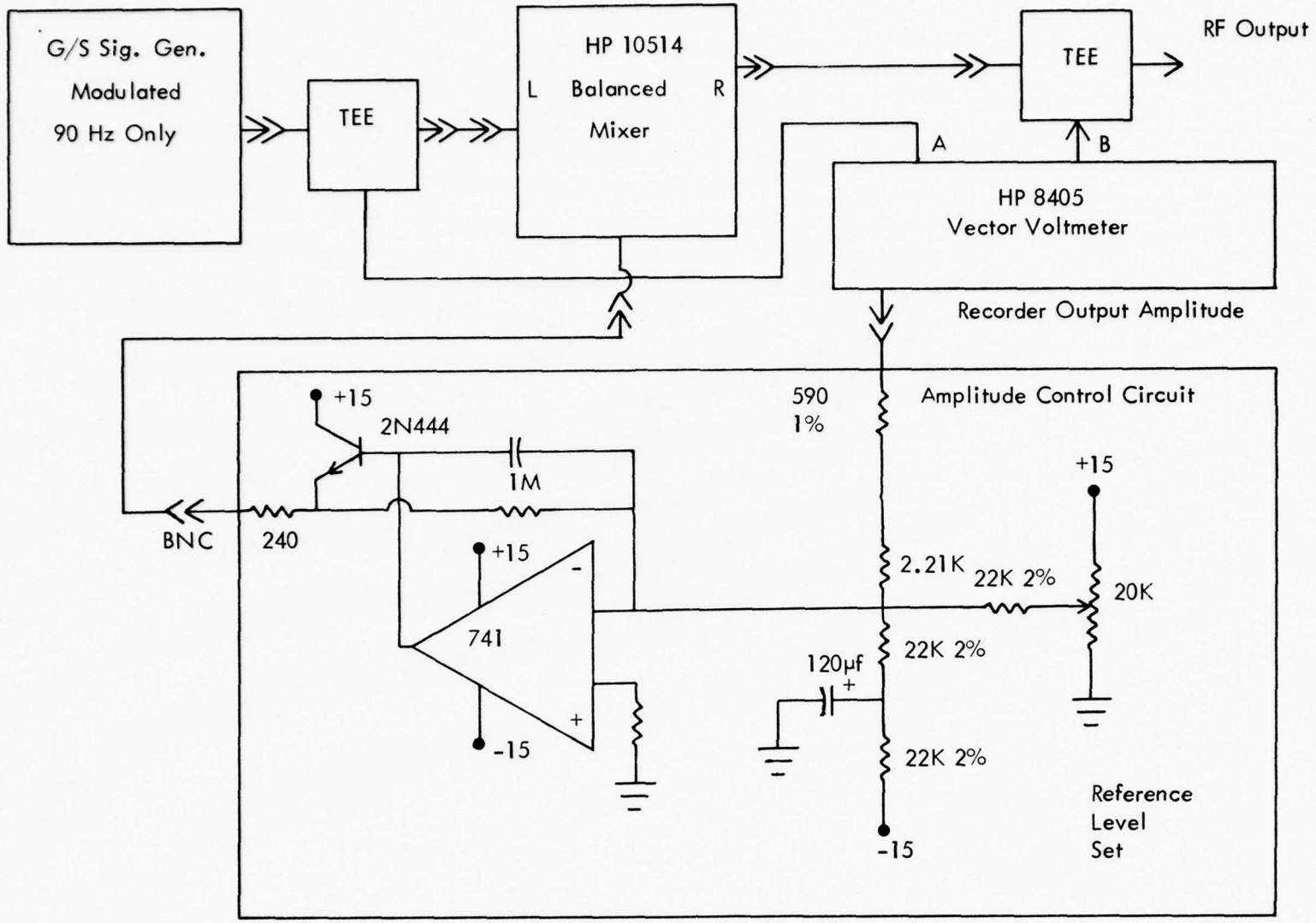

Figure 7. AGC Circuit.

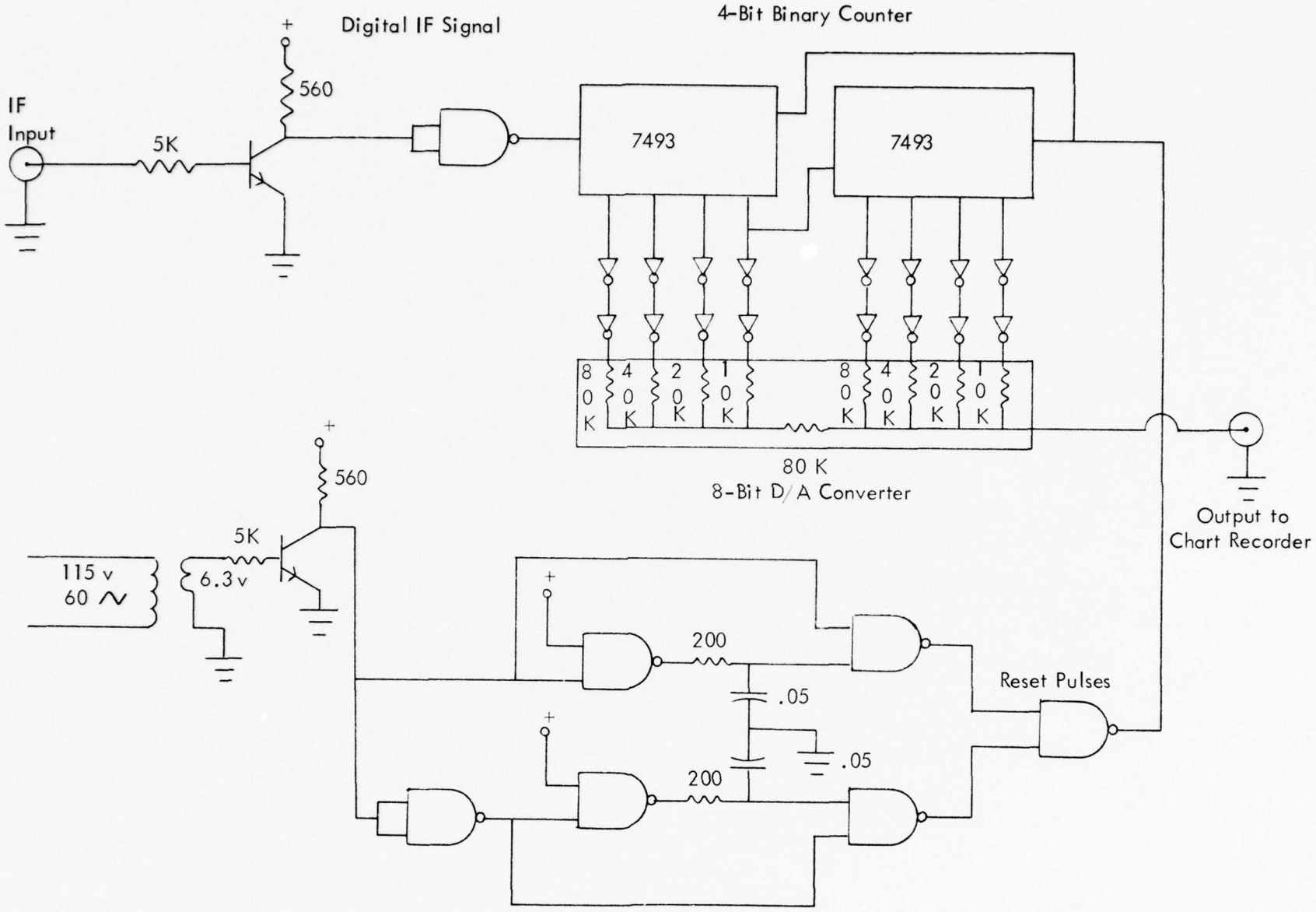

Figure 8. IF Frequency Counter Circuit.

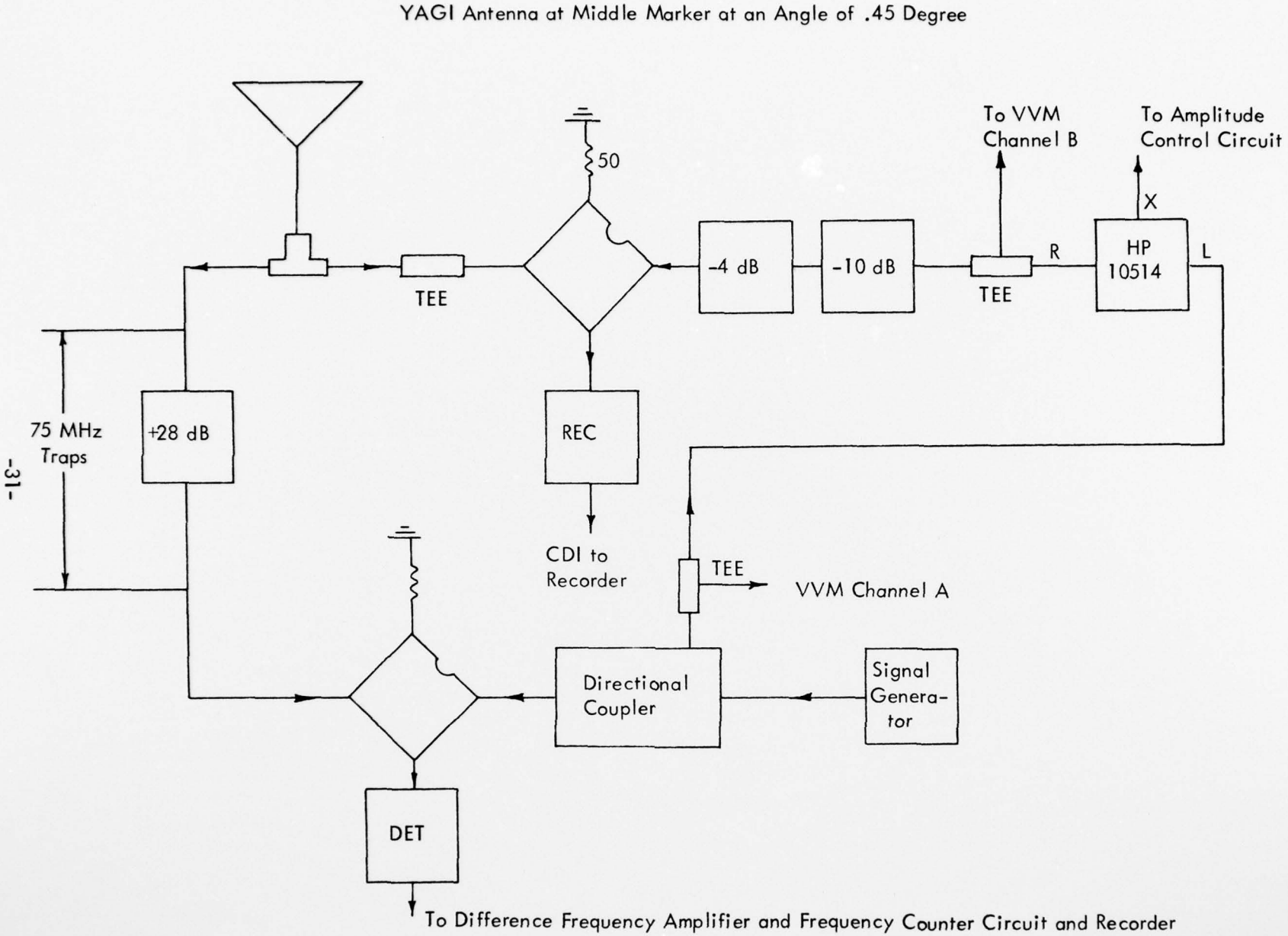

Figure 9. GSCM Monitor - Port Columbus.

$$M_{150} = .635$$

and

$$M_{90} = .165$$

With these values on the input line simulating the received signal, different CDI values were obtained when the modulator motor of the reference generator was quickly switched off and on. Two solutions to this phase problem are the use of phase locking the reference generator audio to that of the transmitted signal or the use of an unmodulated reference signal. While phase locking circuits were being designed, the second method was used so that field tests could be started. With the use of the unmodulated reference source, the CDI output now indicates a higher (150 Hz) positive microampere reading than obtained with the modulated source. However, the CDI output of the receiver still varies significantly as the relative level of the unmodulated reference signal is varied in relation to the level of the received signal.

3. Field Stability Tests - Port Columbus Airport. The system as shown in Figures 7, 8, and 9 was installed at the middle marker location for Runway 10L at Port Columbus Airport for approximately two weeks in November, 1974. Because of the close proximity of the monitor receiving antenna and the marker beacon transmitting antenna, 75 MHz traps had to be installed to eliminate interference from the marker facility (the traps consisted of shorted 50 ohm sections, a half wavelength long at 75 MHz). The receiving antenna was located 4600 feet from the glide-slope transmitting array and was approximately on the extended runway centerline. The receiving antenna, a Yagi with 10 dB gain, was at an angle of 0.46° (36 feet, 7 inches above ground) while the nominal glide-path angle was 2.64°. The ground elevation of both the monitor and transmitting sites was 812 feet MSL.

Over the two week period, the CDI output of the monitor receiver drifted slowly with the maximum shift being 20 microamperes. The chart recordings showed the CDI output would drift slowly from the initial value and then would slowly return. Similarly the chart recordings of the difference frequency showed a change of approximately 4000 Hertz about the initial setting. This drift was clearly temperature dependent as the recordings showed a variation with minimum frequency separation in the early morning hours and maximum frequency separation in late afternoon, repeating each day. However, while the difference frequency varied between 11,000 and 15,000 Hertz, the variations in the CDI were not attributed to this difference frequency change. The CDI variations were most probably due to weather (temperature, rain, etc.) conditions, and any changes in the transmitted signal. In the absence of specific data on the stability of the transmitted signal power or on the weather conditions, no specific conclusions can be drawn from these tests. However, from the results of these stability tests it would appear that this capture monitor will be able to detect signal level changes due to changing ground level under snow cover.

4. Field Test - Tamiami, Florida. Following the stability tests at Port Columbus Airport, the GSCM was reworked to remove excess connectors and cables to improve reliability. The system was then taken to the Tamiami Airport, Miami, Florida for further field testing. A null reference glide slope was used for these tests with antenna heights of 35.25 feet and 17.625 feet for the sideband and carrier antennas respectively. At 333.2 MHz this gives a 2.4 degree glide path. This with a 0.1 degree upslope of the ground would give a 2.5 degree path measured in the air.

The GSCM was located 2000 feet from the transmitting antennas and on the runway centerline. The initial height of the GSCM receiving antenna was 14 feet. To simulate a changing ground plane height, due to snow accumulation, the two transmitting antennas and one monitor antenna (see Figure 10) were lowered in one foot increments until a total change of six feet was achieved (data at the 5-foot point was not taken). Data as taken by the GSCM, the path angle and lower width angle as measured by Ohio University flight check aircraft and theodolite reference are reported. For analysis, the measured angle values are compared with calculated values of the path and width angles for the respective antenna heights, while the GSCM data are compared with data obtained from a controlled laboratory simulation using the GSCM setup and a second signal generator to simulate the received signals for the respective antenna heights.

Table 9 lists the glide-slope path angle, the lower width angle (150μa; 150Hz), and the lower path width as calculated and as measured by the flight check aircraft for the transmitting and receiving antenna height changes listed (antennas were lowered). The flight checks were performed on two consecutive days. The theoretical values listed were calculated assuming that the initial transmitting antennas were set for a 2.4 degree path angle with sideband power set for a 1.4 degree path width (± 150 microamperes). A 0.1 degree angle, corresponding to the upslope of the ground plane, was then added to the theoretical angles so that they agree with the angles as measured by flight checks.

An examination of the data in Table 9 shows that the measured values from the first flight checks agree closely with the theoretical values except the lower width angle for the 6-foot antenna change. For antenna changes of 0 to 4 feet, both the path angle and lower width angle rose, and the lower path width narrowed (sharpened). But in lowering the antennas an additional 2 feet, for a total change of 6 feet, the path angle rose but the lower width angle dropped producing a very broad lower path width which is anomalous and unexplained.

The second flight check data, which included data only for antenna height changes of from 0 to 3 feet, agrees with the theoretical values within .05 degree or better. While the path angle taken on different days agrees within .01 degree (except at the 2-foot antenna height change), the lower width angle and, consequently, the lower path width show differences of as much as .08 degree when antenna height changes are made.

Table 10 and Figure 11 present the field measured, and laboratory simulated, values of the GSCM CDI output for antenna height changes of from 0 to 6 feet. The field

Figure 10. Use of Clark Tower for Elevating Probe Antenna Used in Tests Simulating Ground Plane Elevation Changes Due to Snow.

Antenna Height Change (Feet)	Theoretical		Flight Checks					
			First			Second		
	Path Angle (Degrees)	Lower Width Angle (Degrees)	Path Angle (Degrees)	Lower Width Angle (Degrees)	Lower Path Width (Degrees)	Path Angle (Degrees)	Lower Width Angle (Degrees)	Lower Path Width (Degrees)
0	2.50	1.80	2.52	1.76	.76	2.52	1.75	.77
1	2.57	1.86	2.61	1.87	.74	2.60	1.90	.70
2	2.64	1.93	2.69	1.97	.72	2.64	1.90	.74
3	2.72	2.00	2.73	2.03	.70	2.73	1.95	.78
4	2.81	2.08	2.81	2.12	.69	----	----	----
6	2.99	2.26	2.98	2.05	.93	----	----	----

Table 9. Comparison of Theoretical and Measured Path and Width Angle Information.

Antenna Height Change (Feet)	GSCM CDI OUTPUT	
	Simulated	Field
0	0	0
1	45	36
2	101	97
3	153	165
4	195	213
5	237	---
6	275	269

Table 10. Comparison of Simulation and Field Test GSCM CDI Values.

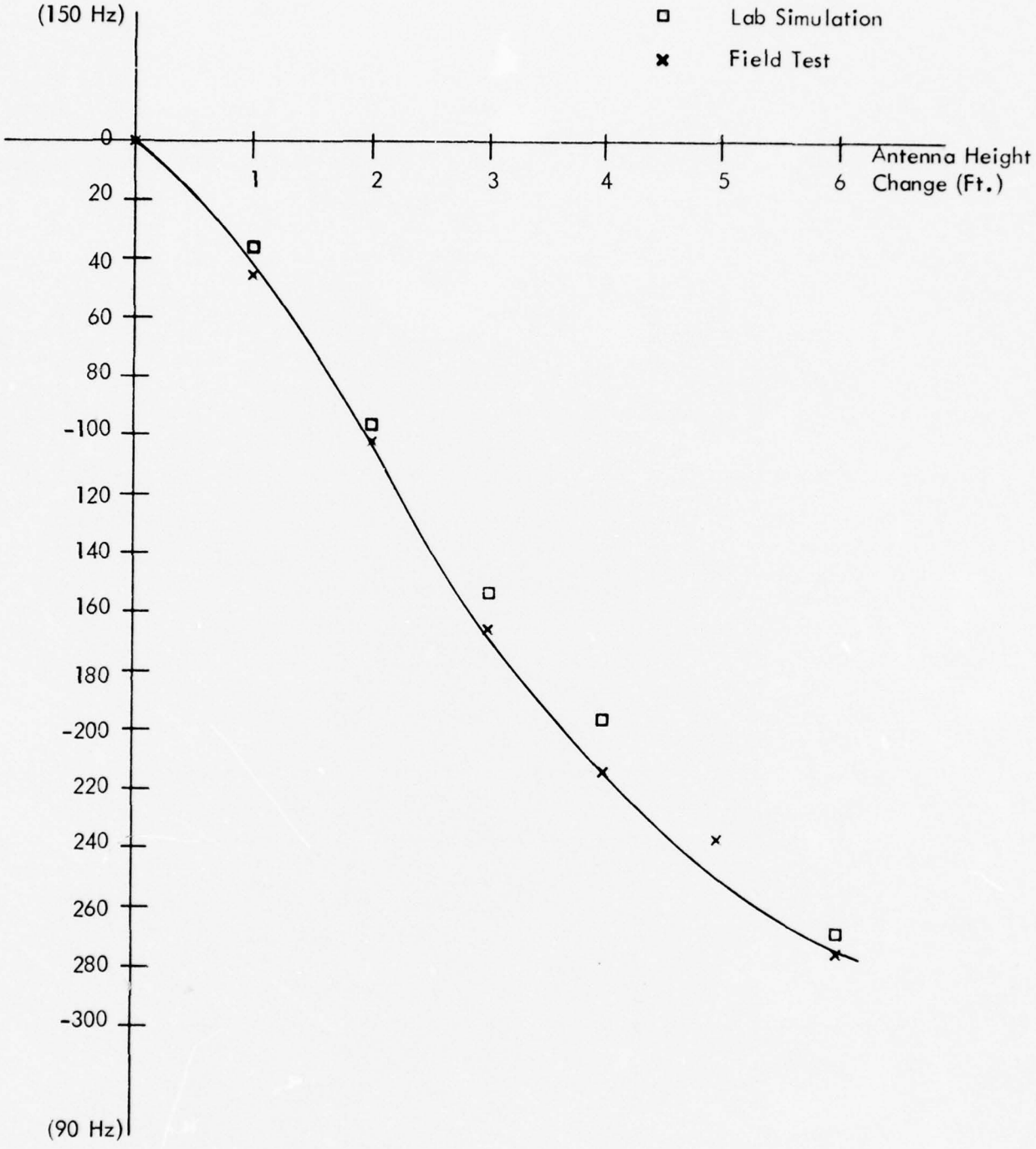

Figure 11. GSCM Response Comparing Field Measurements to Simulation Measurements.

data, as well as the flight check data above, was obtained using a Wilcox solid state glide-slope transmitter producing a carrier power of three watts. The transmitter frequency was 333.198715 MHz, while the reference generator frequency was 333.188378 MHz, giving a difference frequency of 10.337 KHz. An examination of the data in Table 10 and Figure 11 shows very good agreement between the field and laboratory data.

The RF signal strength was also measured during the field tests using a Cardion field detector connected to the +10 dB Yagi receiving antenna. The field strength values were obtained using a TU-4 glide-slope transmitter producing a carrier power of 4.5 watts at 331.1 MHz. The TU-4 transmitter was used as crystals were not available to use the Cardion on the Wilcox frequency. Table 11 lists the measured RF signal strength and the calculated signal strength (as equated to the initial measured value), and the two sets of data agree very closely.

Antenna Height Change (Feet)	Measured Signal Strength (Microvolts)	Calculated Signal Strength (Microvolts)
0	3200	3200
1	2700	2816
2	2400	2432
4	1800	1792
6	1200	1216

Table 11. Signal Strengths for Various Antenna Heights.

5. Laboratory Simulation. In order to have a basis upon which to compare the data taken during the Tamiami tests, a laboratory simulation of the field tests was run on the GSCM. Figures 12 and 13 show the setup for the simulations. For each simulated antenna height, a signal strength and DDM was calculated and set up on the Boonton 232-A signal generator which simulated the received signal. A computer program provided the signal strength, DDM and CDI values which should be present for the various antenna height settings. Also included in the simulation were the cases where the sideband power from the transmitter is changed by ±20% and where the phase of the 90 Hz reference audio is changed with respect to the phase of the 90 Hz audio from the simulated received signal. The various parameter values used in the laboratory simulation are listed in Table 12. As can be seen, high values of DDM are encountered in this simulation, values which the Boonton 232-A will not readily produce. This necessitated the use of the high DDM circuit shown in

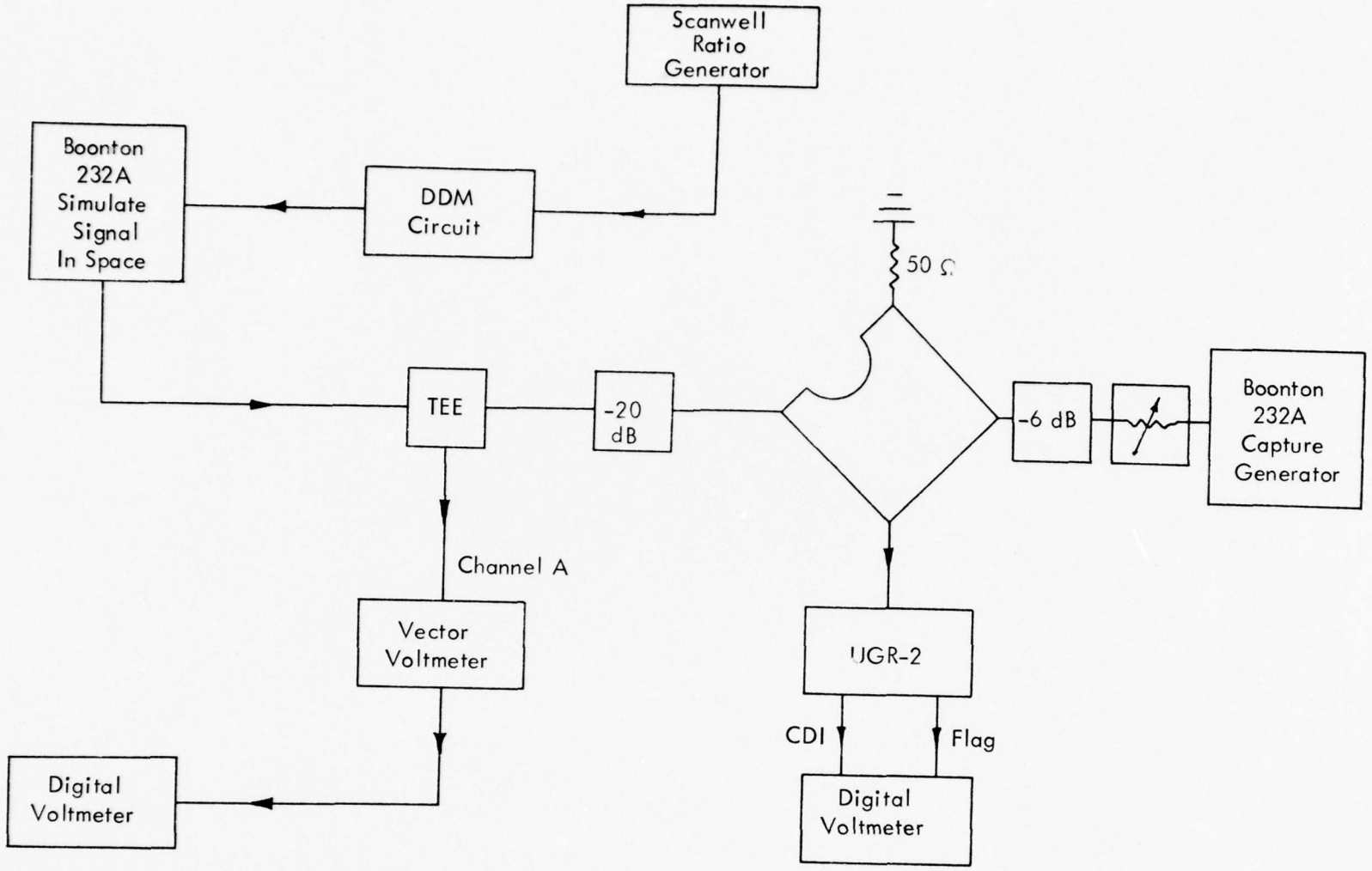

Figure 12. Test Setup.

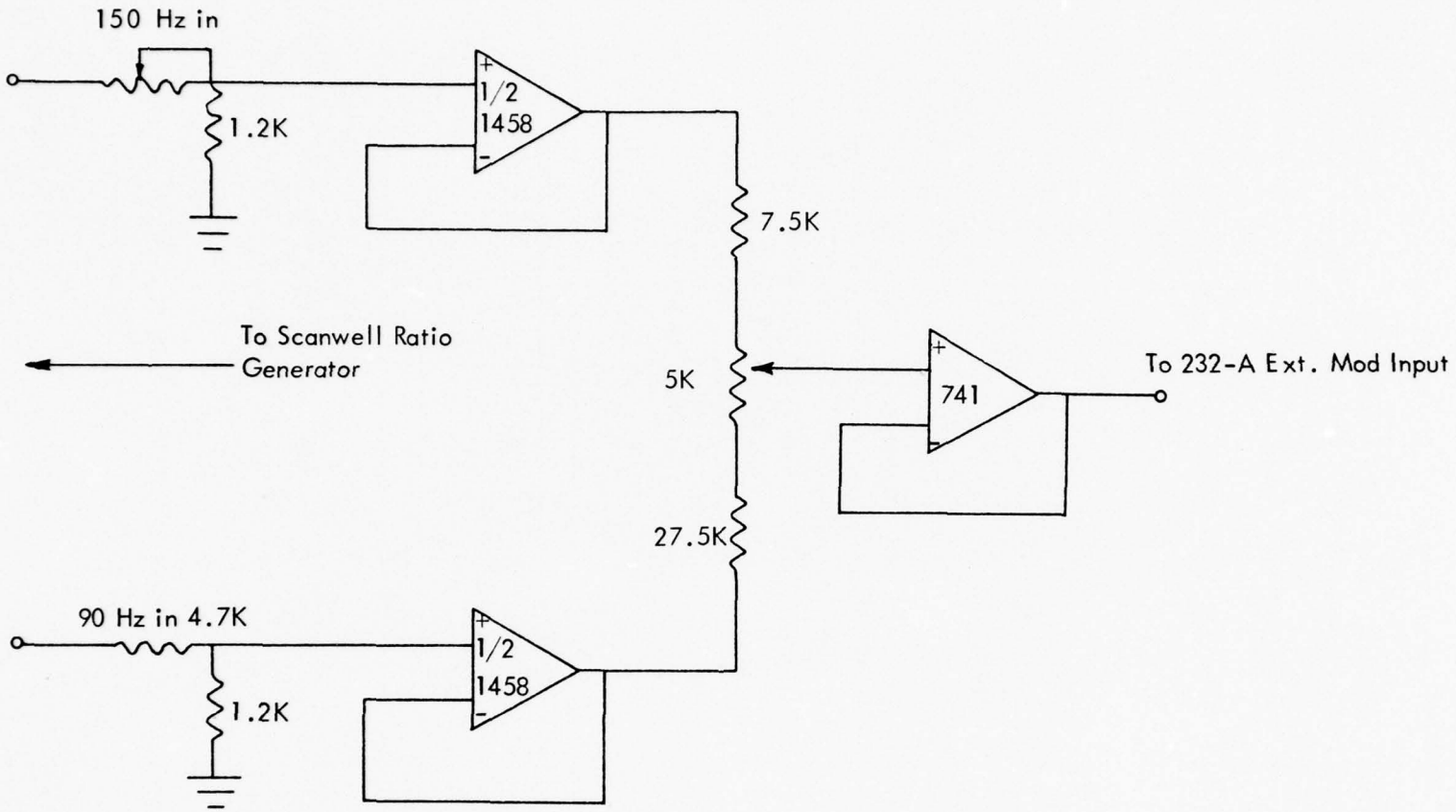

Figure 13. High DDM Circuit.

Change in Height	"A" Ratio	DDM	CDI	Field Strength
0	.247	.380	326.	1.00
	.221	.340	292.	
	.271	.417	358.	
1	.247	.395	339.	.87
	.221	.354	303.	
	.271	.434	372.	
2	.247	.410	352.	.76
	.221	.367	315.	
	.271	.450	386.	
3	.247	.429	368.	.65
	.221	.384	329.	
	.271	.471	403.	
4	.247	.445	382.	.55
	.221	.399	342.	
	.271	.488	419.	
5	.247	.466	400.	.46
	.221	.417	358.	
	.271	.511	438.	
6	.247	.486	417.	.38
	.221	.436	373.	
	.271	.533	457.	

Table 12. Calculated DDM, CDI, and Field Strength for Each Antenna Height and for Three "A" Ratios.

Figure 13. The 90 and 150 Hz audio signals needed are obtained from the 90 and 150 Hz filter outputs of a Scanwell Ratio Generator.

The values of RF signal level were measured using an HP 8405 Vector Voltmeter with a digital voltmeter connected to the recorder output of the vector voltmeter. The various attenuator pads in the circuit (See Figure 12) were needed to provide isolation between the two generators.

A comparison of field-measured data with laboratory-simulated data, which was discussed previously in connection with the values shown in Figure 11 and Table 10, indicated good agreement between the two sets of data.

Figure 14 shows the CDI output from the GSCM with the sideband power (the "A" ratio in Table 12) setup for a normal course width ("A" = .247) and for an increase ("A" = .271) and decrease ("A" = .221) of sideband power by 20%. The CDI values for the antenna height changes of 5 and 6 feet, with "A" = .271 could not be obtained as the required DDM values were beyond the range of the high DDM circuit. However, the results shown in Figure 14 indicate that the GSCM CDI output is sensitive to changes in the sideband power, especially when the received and reference signal levels are approximately equal, which gives a CDI output value near zero. With the reference signal level set so that the CDI output was zero, increasing, then decreasing, the sideband power produced a CDI output reading of +16 and -18 microamperes respectively.

The sensitivity of the CDI output to a change in phase of the 90 Hz audio modulating the reference generator is shown in Figure 15. The test was initially set up with the 90 Hz reference generator modulation in phase with the 90 Hz (simulated) glide-slope signal modulation. The RF level of the reference generator was set to give initially a zero CDI output. The phase of the reference generator audio was then changed with respect to the glide-slope 90 Hz audio phase and the corresponding CDI recorded. The phase angles were measured by displaying the two audio signals on a dual channel oscilloscope. From the results shown in Figure 15, it appears that a phase error of about 16 degrees may be tolerated with only a one microampere CDI error. The amount of CDI error incurred depends upon how much 90 Hz audio is present in the glide-slope signal, that is, if there were no 90 Hz audio in the glide-slope signal, the phase of the 90 Hz audio in the reference generator would not matter. This test was performed with a glide-slope signal (simulated) of 0.3 DDM, which has a higher level of 90 Hz audio than would be found at typical monitor points in actual field use. Table 12 lists the DDM as being 0.38 under normal conditions for a glide slope set for a 2.5 degree path angle and 1.4 degree path width. Thus the values shown in Figure 15 are slightly conservative. However, it appears that the 90 Hz audio of the reference generator will have to be phase-locked to that from the glide-slope signal to insure proper GSCM operation.

6. Statement of Future Work. The above sections presented the results of a study to develop a far-field glide-slope monitor that operated on capture effect principles. Preliminary results of laboratory and field tests have been presented. This concluded the work on the GSCM that was performed under the contract DOT-FA69WA-2066,

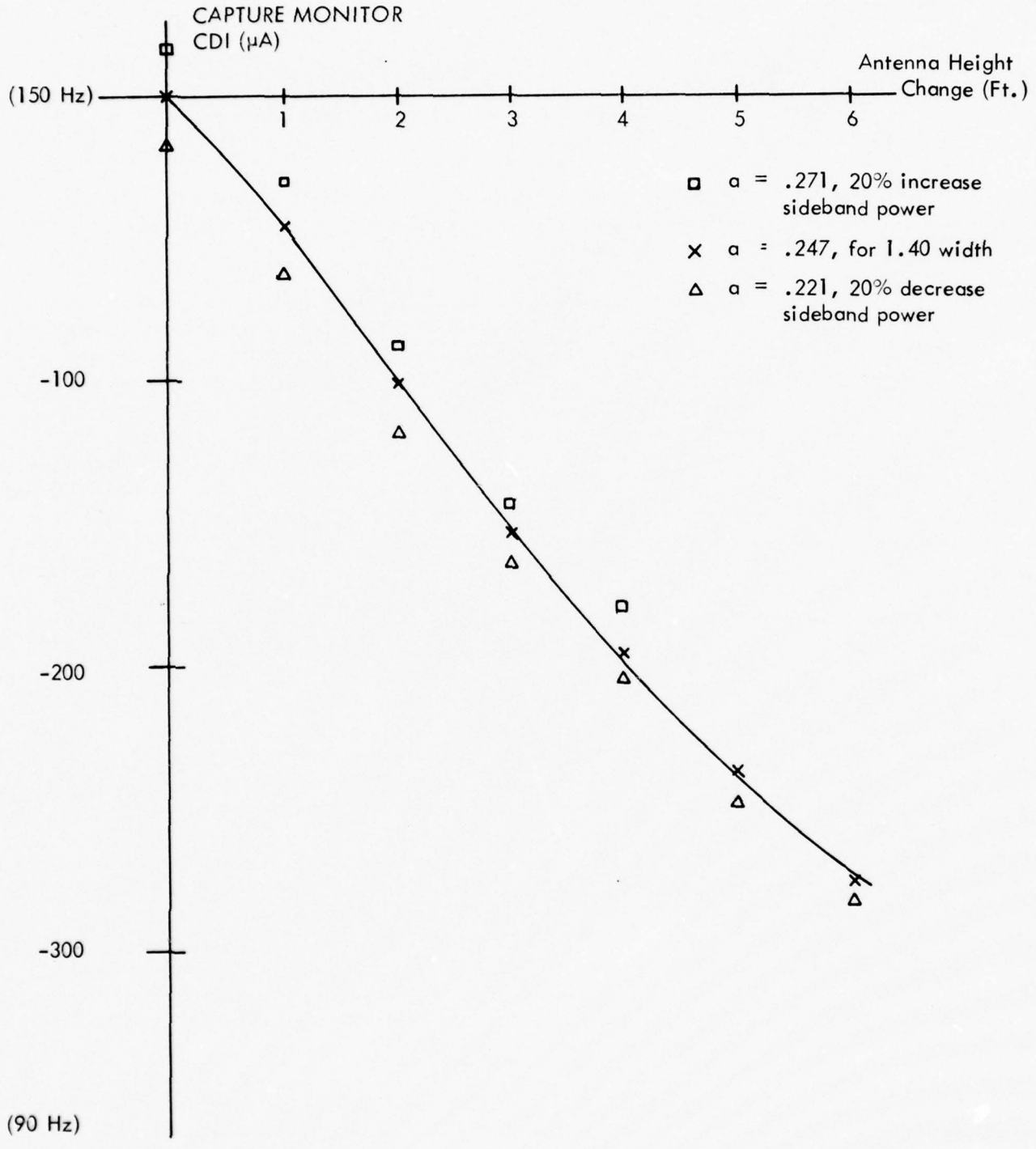

Figure 14. GSCM Response for Three Values *of the Sideband Power Ratio.*

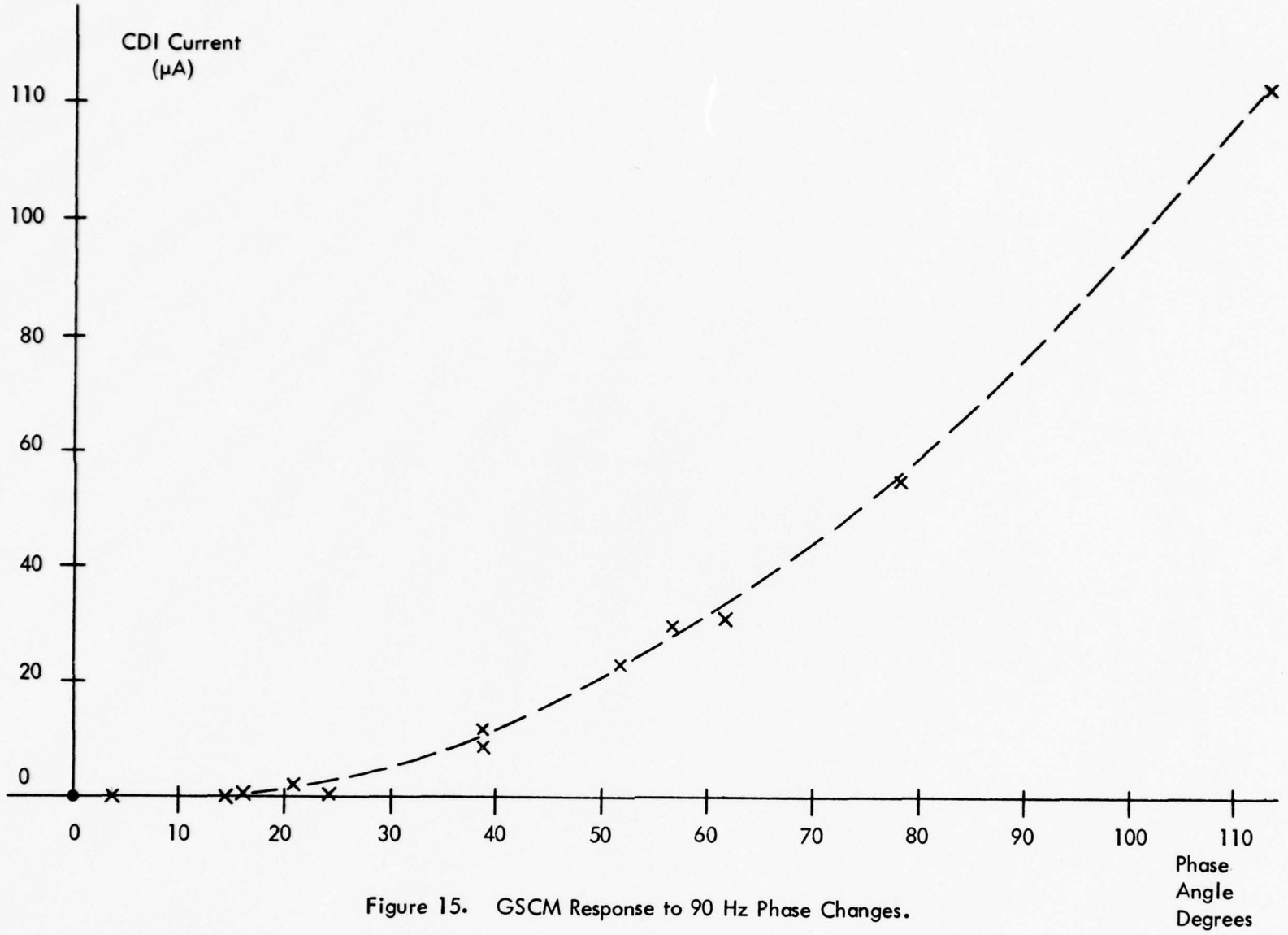

Figure 15. GSCM Response to 90 Hz Phase Changes.

Modification 16. The GSCM will undergo further development under Contract FA75WA-3581, the first step of which was the installation of the GSCM at Houghton County Airport, Houghton, Michigan for testing under snow conditions.

IV. ACKNOWLEDGEMENTS

Dr. M. J. Stefanik performed the engineering analysis work associated with the gradient clearance monitor. Messrs. Jack McDonald, Lewis Drake, and Joe Battistelli provided necessary engineering assistance.

Mr. Robert Rondini and Mr. Larry Mitchell performed the engineering work reported for the two-frequency, capture-type far-field monitor. These men with Dr. P. H. Garrett and Mr. Dave Putnam produced the space modulation quotient monitor.

Messrs. Harry Hooghkirk, Richard Zoulek, and Jack Morehart were responsible for the field data collected on the far-field gradient type monitor.

Professor G. E. Smith served as consultant and editor of this report while Ms. Hope Mills was editorial coordinator. Dr. Richard McFarland was project director.

Appreciation is extended to Dr. Godfrey Lucas and the Air Navigation Group at the University of Sydney, Australia for their assistance in scale model measurements.

V. REFERENCES

[1] Stefanik, Michael J.,"Instrument Landing System Improvement Program, Gradient Clearance Monitor Final Report,"FA-RD-72-147, Avionics Engineering Center, Department of Electrical Engineering, Ohio University, Athens, Ohio, October, 1972.

[2] "Instrument Landing System Glide Slope," Manual No. FV-301, Department of Transportation, Federal Aviation Administration, Aeronautical Center, FAA Academy.

[3] "United States Standard for Terminal Instrument Procedures (TERPS)," Second Edition, Department of Transportation, Federal Aviation Administration, February, 1970.

[4] "Amplitude Modulation," Manual No. FV-106-1, Department of Transportation, Federal Aviation Administration, Aeronautical Center, FAA Academy, February, 1971.

[5] Butts, H. H., "Reno, Nevada Glide Slope Evaluation Tests (November 13-24, 1961) Utilizing Capture Effect Principles in Conjunction with M-Array Systems," Federal Aviation Administration, February 6, 1961.

VI. APPENDICES

APPENDIX A. OPERATION AND MAINTENANCE INSTRUCTIONS FOR OHIO UNIVERSITY SPACE MODULATION QUOTIENT MONITOR

1. GENERAL DESCRIPTION

a. The Space Modulation Quotient Monitor. The Space Modulation Quotient (SMQ) Monitor extracts the desired path information from the composite audio. With one notable exception, the SMQ is a precision version of the audio section of a standard localizer or glide-slope receiver. The 90 and 150 Hz audio are separated with bandpass filters (BPF), and the individual audio voltages are rectified. The rectified audio is low-pass filtered, and the DC components are subtracted to yield the audio difference signal. The unique part of the SMQ is the analog divider at the output. At this point the sum of the DC components is divided into the difference of the DC components. This operation makes the output independent of the amplitude of the composite and sensitive only to the relative amplitudes of the 90 and 150 Hz DC components. This means any drift in gain of any circuit before the SMQ will not change the SMQ output. It should be noted that this also makes the SMQ insensitive to a change in percent modulation of the transmitter. Percent modulation, however, is monitored by the integral monitor and this parameter may be taken into account in that subsystem. See Figures A-1 and A-2 for photographs.

The first stage is a buffer amplifier to provide a high input impedance to the audio source. See Figure A-3a for converter schematic and Figure A-3b for calibrator schematic. The next stage provides gain which can be adjusted so that the circuits which follow are operating in the best dynamic range for the components. The next stage is a phase shifter to compensate for the difference in phase shift through the filters. This merely allows visual comparison of the sum of the outputs of the filters with the input on an oscilloscope trace. The filters are specially ordered active filters from Burr Brown Research Corporation. They are four pole stagger tuned filters with a $Q = 10$ and maximally flat in the passband. The 90 and 150 Hz signals now separated can be rectified and low-pass filtered. The rectification is done with an absolute value circuit. This is shown in Figure A-4.

The circuit used combines the absolute value operation and low-pass filtering into one operation. Without the capacitor the circuit would be an absolute value circuit. The absolute value function results in a full wave rectified sine wave and the LPF provides the DC level of this wave with the AC components attenuated. The -3dB corner frequency for the LPF is approximately 1 Hz. The time constant is approximately 0.2 second. The DC levels proportional to the 90 and 150 Hz signals are now subtracted in a differential amplifier. The sum is divided into the difference in an analog divider and the output from the divider is scaled such that the digital panel meter reading is equivalent to SMQ current in microamperes in a standard 1000 Ω CDI. The output is presented on an Analog Devices digital panel meter. The SMQ monitor can be switched to read the values of CDI current from either a localizer receiver or a glide-slope receiver. The calibrate mode provides either a 0, -90, or +90 indication on the digital panel meter. The SMQ signal also goes to output jacks for chart recorders and comparators.

b. Adjustment and Calibration. The SMQ Meter has adjustment procedures for localizer, glide slope, and calibrator. These adjustments are best done in the order stated and should be done carefully to achieve accurate results with the SMQ. The SMQ should warm up for two hours before adjustment. Refer to Figure A-1 for external adjustments and Figure A-5 for internal adjustments and key to test point functions.

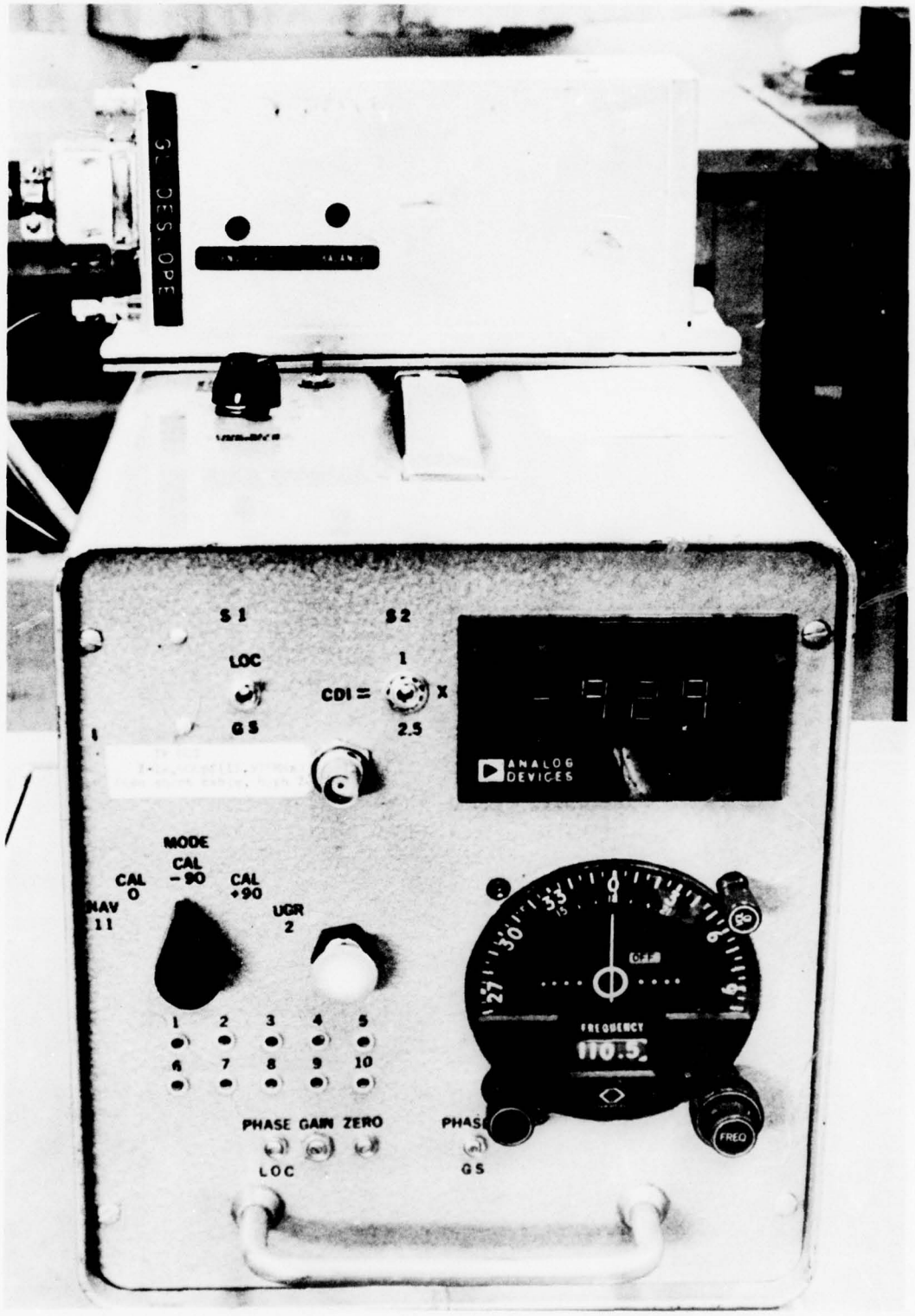

Figure A-1. Precision Localizer and Glide-Slope Monitor - Front View.

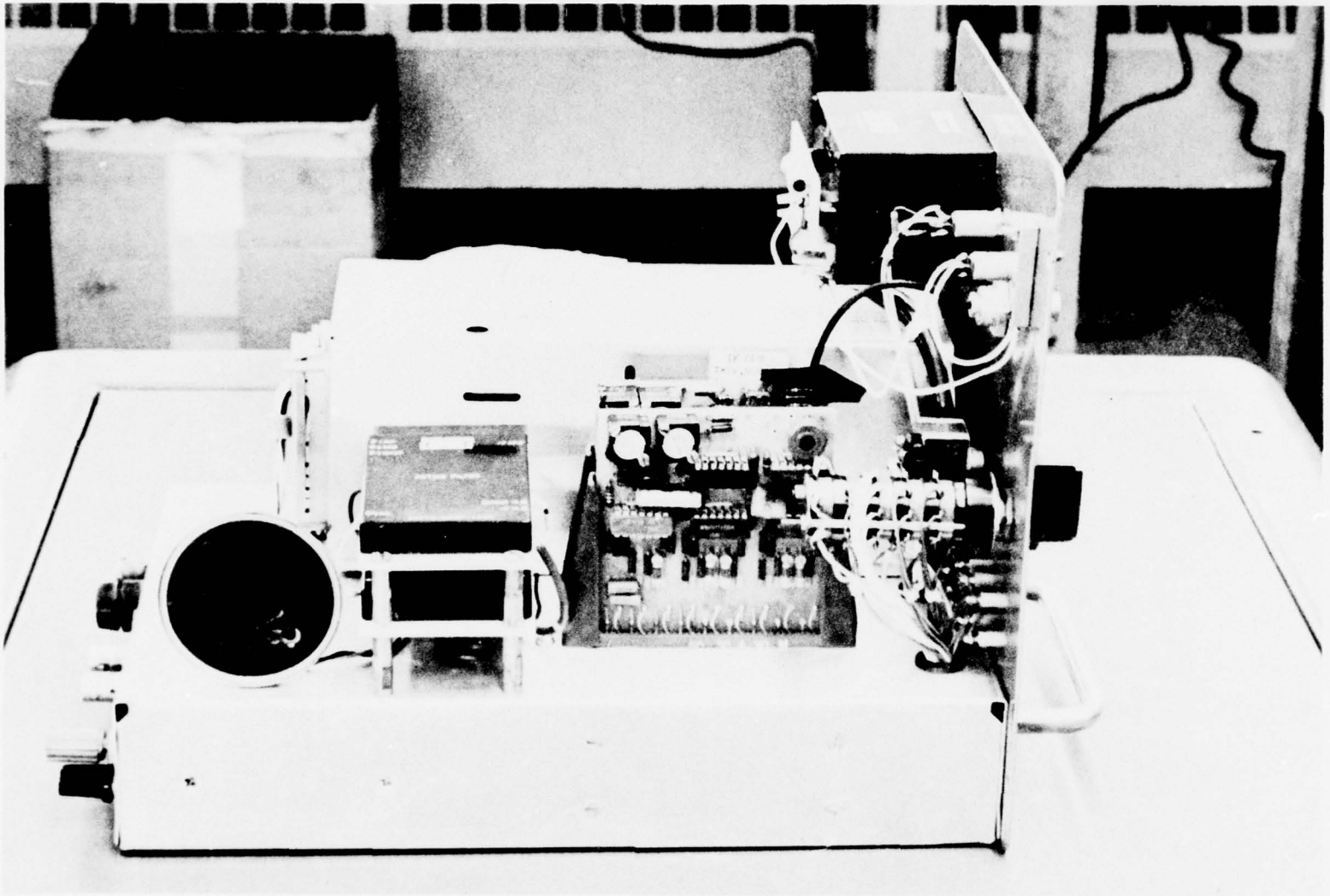

Figure A-2. Precision Localizer and Glide-Slope Monitor - Inside View.

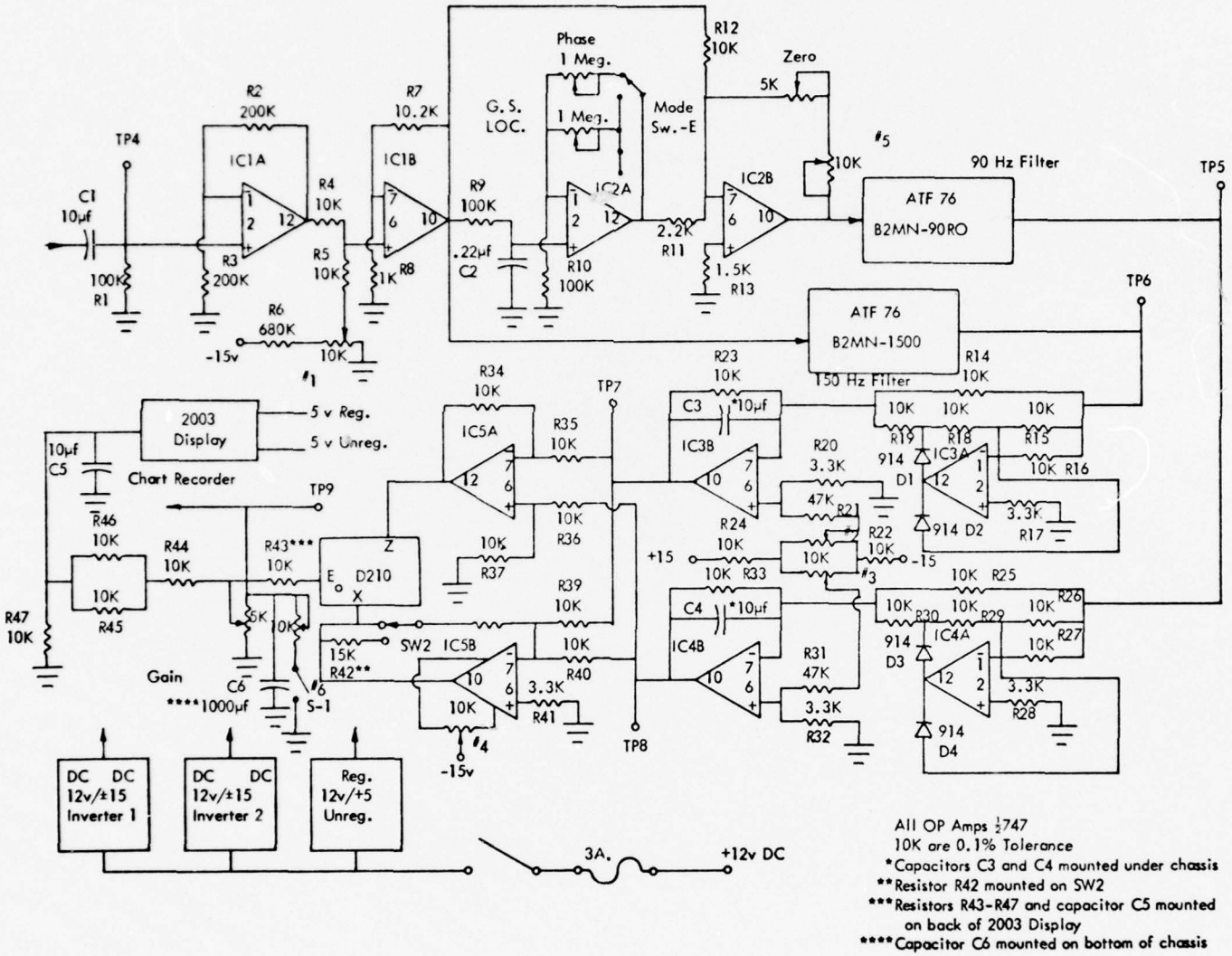

All OP Amps ½747
10K are 0.1% Tolerance
*Capacitors C3 and C4 mounted under chassis
**Resistor R42 mounted on SW2
***Resistors R43-R47 and capacitor C5 mounted on back of 2003 Display
****Capacitor C6 mounted on bottom of chassis

Figure A-3a. 90/150 Converter.

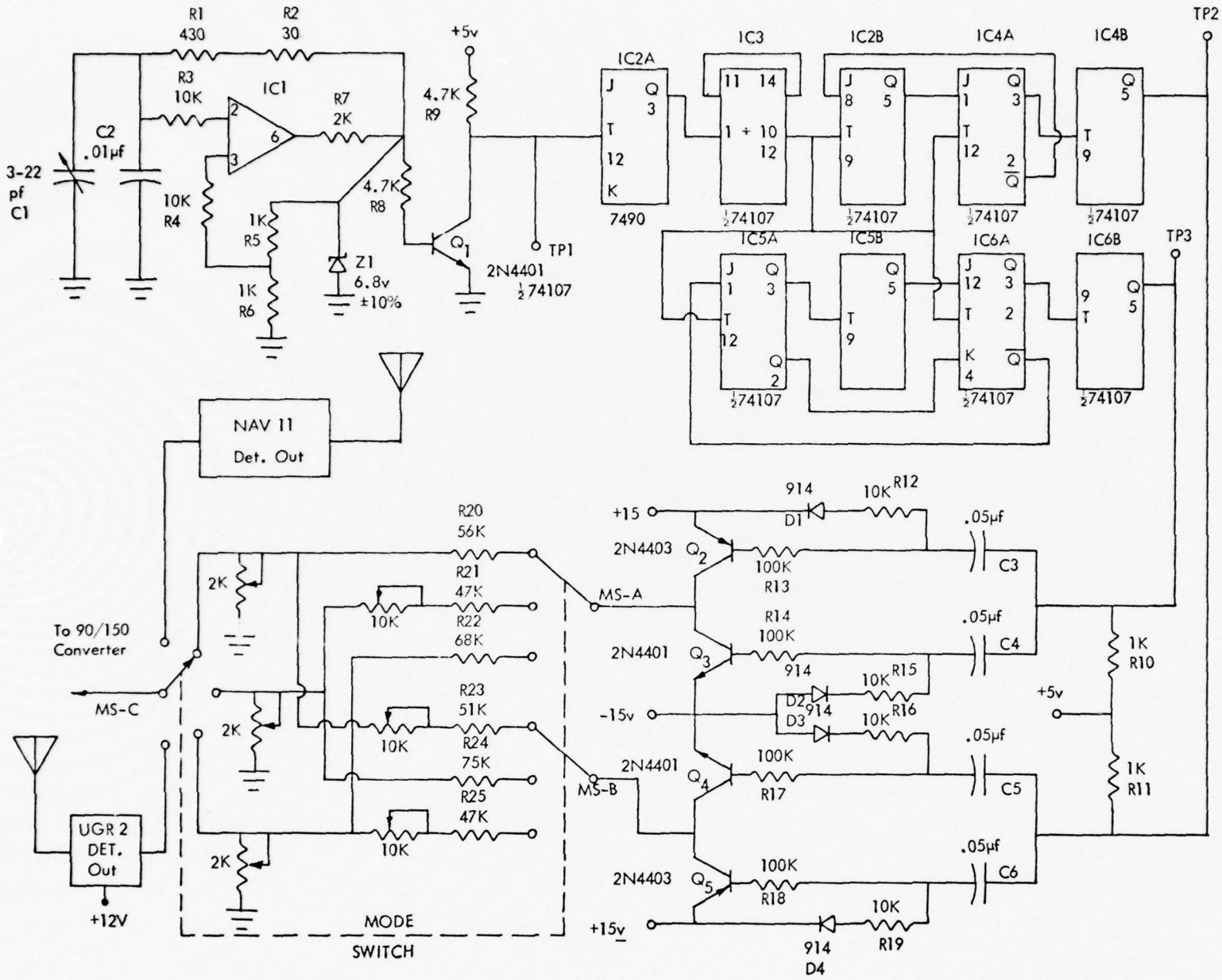

Figure A-3b. Transfer Standard Calibrator (Circuit Diagram).

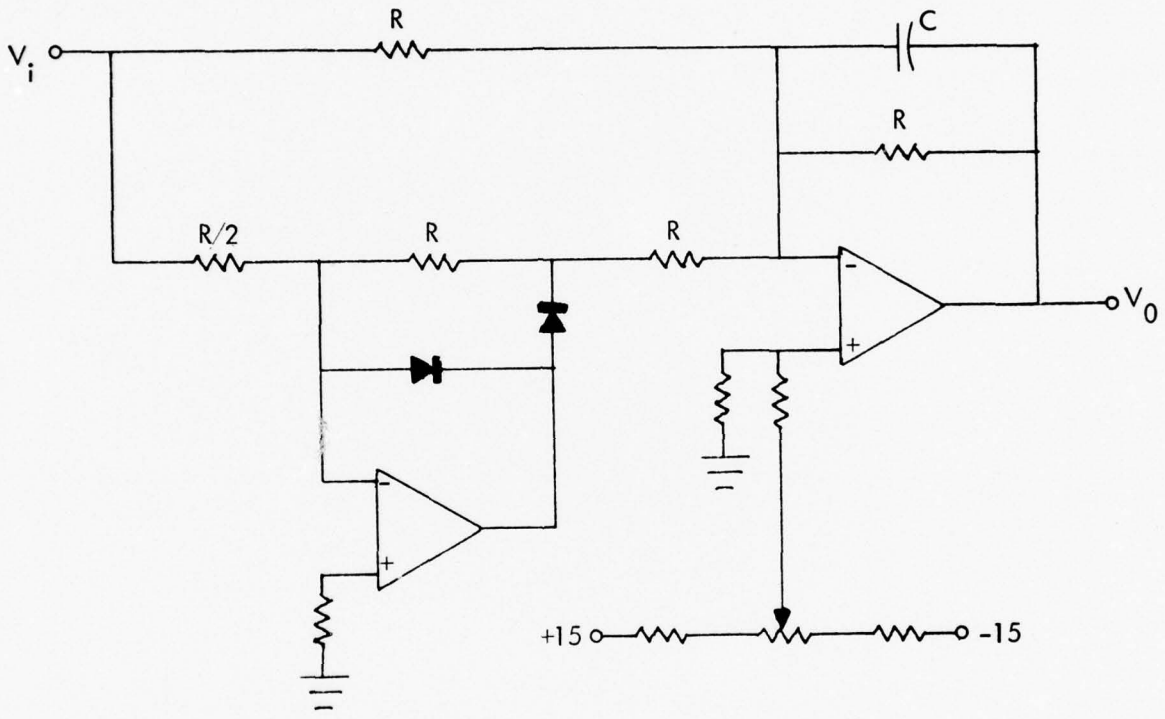

Figure A-4. Absolute Value Circuit.

$$V_0 = \frac{|V_i|}{RCs + 1}$$

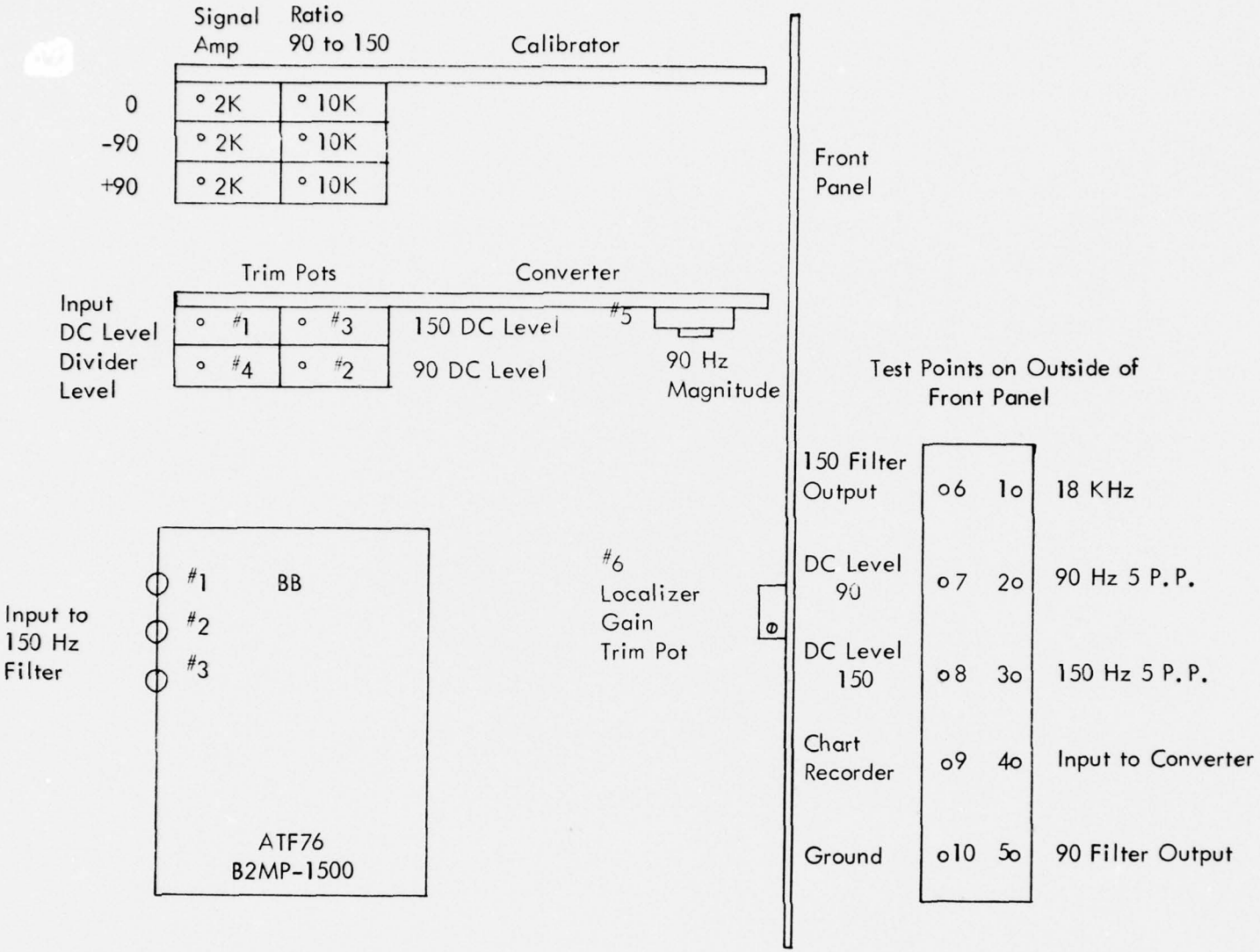

Figure A-5. Trim Pot and Test Point Locations.

c. Processor Adjustments.

1. MODE: NAV 11, S1: LOC, S2:1, Localizer Receiver: OFF.

2. Short TP-4 to TP-10 (ground).

3. Connect VTVM to Pin 3 of 150 Hz filter.

4. Adjust Pot No. 1 for zero volts at Pin 3 of the 150 Hz filter.

5. Adjust Pot No. 3 for zero volts at TP-7.

6. Adjust Pot No. 2 for zero volts at TP-8.

7. Remove short from TP-4 to TP-10.

8. Turn Localizer Receiver - ON, connect properly adjusted localizer generator to NAV 11 input (on back of chassis).

9. Connect a dual trace oscilloscope with one channel at TP-5 and the other channel at TP-6.

10. Adjust Pot No. 5 so that the peak-to-peak amplitude at the 90 Hz filter output is identical to that at the 150 Hz filter output.

11. Connect resistor network between TP-5, TP-6, and TP-10 (see Figure A-6).

12. Connect one channel of the oscilloscope to TP-4 and the other channel to the junction of the resistor network.

13. Set the localizer generator TONE RATIO to "0 dB" and obtain a modulation pattern on the oscilloscope.

14. Adjust PHASE LOC such that the peaks of the pattern from the resistor network junction are in the same relation as the peaks of the pattern from TP-4 (see Figure A-8).

15. Adjust ZERO to converge the pattern (see Figure A-8).

16. Connect a properly adjusted glide-slope generator to the UGR-2 input (on UGR-2 receiver).

17. Set the glide-slope generator TONE RATIO to "0 dB".

18. Set MODE: UGR-2, S1: G S, S2:1.

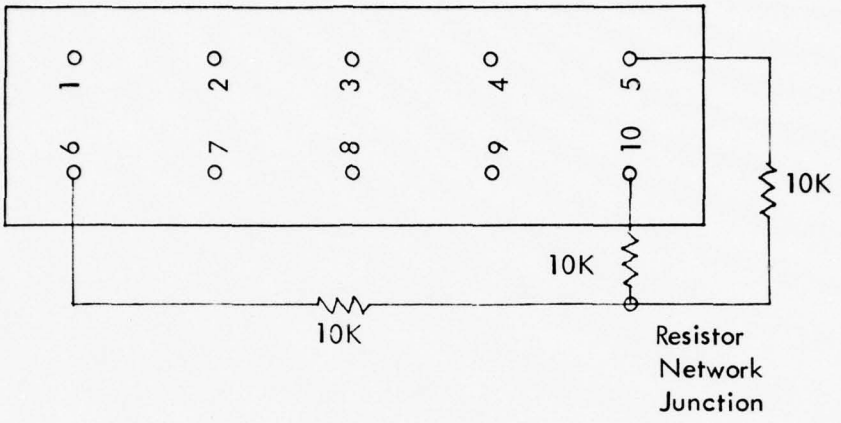

Figure A-6. Test Resistor Network.

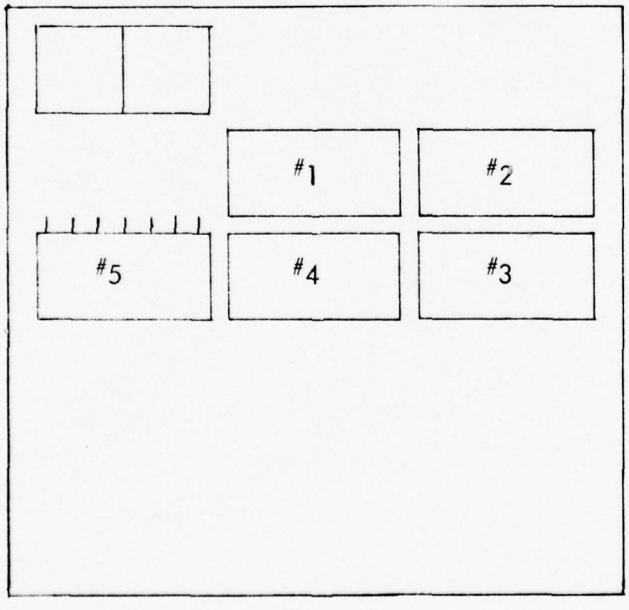

Figure A-7. Processor Circuit Board - IC Locations.

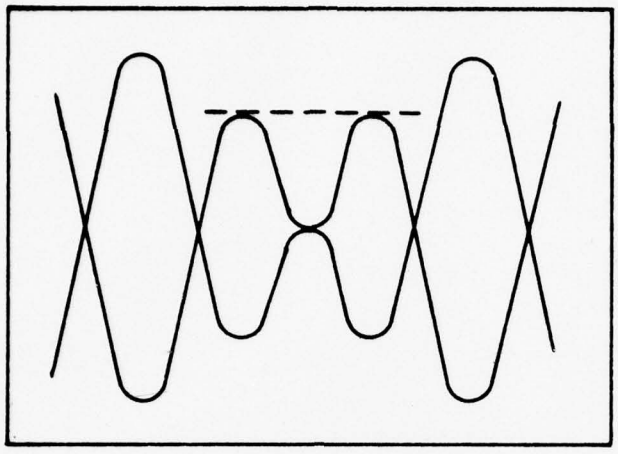

Modulation Pattern from TP-4.

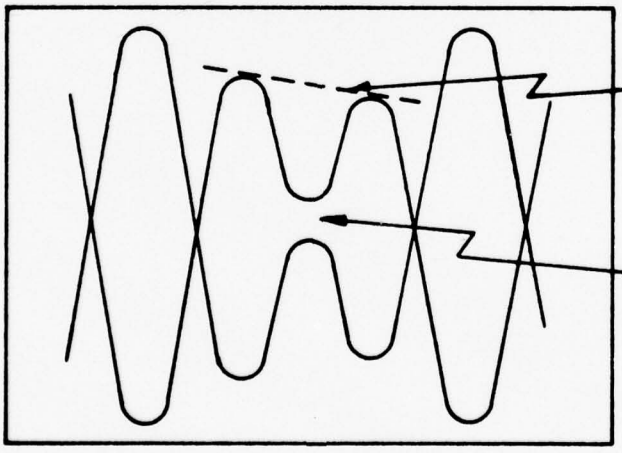

Modulation Pattern from Junction of Resistor Network.

Figure A-8. Oscilloscope Patterns for Proper Adjustment of the Phase and Zero Controls.

19. Repeat step 14 for the PHASE G S control.

20. With the VTVM, measure the voltage at TP-7 and TP-8. Adjust Pot No. 4 so that the voltage at Pin 10 of IC No. 5 (see Figure A-7) is the negative of the sum of the voltages at TP-7 and TP-8. That is, $V_{tp-9} = -(V_{tp-7} + V_{tp-8})$.

21. Recheck the PHASE G S and ZERO controls to get a reading of zero on the Digital Panel Meter (DPM).

22. Set the glide-slope generator TONE RATIO to 3.3 dB (150 Hz). Adjust the GAIN to get a reading of 127 on the DPM.

23. Set the TONE RATIO to 3.3 dB (90 Hz). The DPM should read -127.

24. Set MODE: LOC, S1: LOC, S2:1.

25. The DPM should read approximately 0. If not, slightly readjust PHASE LOC to get a reading of 0.

26. Set the localizer generator TONE RATIO to 4 dB (150 Hz). Adjust Pot No. 6 (inside front panel-see Figure A-5) to get a reading of +90 on the DPM.

27. Set the TONE RATIO to 4 dB (90 Hz). The DPM should read -90.

d. Calibrator Adjustments.

1. Set MODE:LOC, S1:LOC, S2:1, localizer generator TONE RATIO: 0 dB.

2. Note the peak-to-peak amplitude at the resistor network junction on the oscilloscope.

3. Set MODE:CAL-0.

4. Adjust SIGNAL AMP - 0 (2K Pot - see Figure A-5) to get approximately the same peak-to-peak amplitude on the oscilloscope as recorded in Step 2.

5. Adjust RATIO 90 to 150 - 0 (10K Pot) to get a reading of zero on DPM.

6. Set MODE: CAL -90.

7. Adjust SIGNAL AMP : -90 to get peak-to-peak amplitude as in 2 above.

8. Adjust RATIO 90 to 150 : -90 to get a reading of -90 on DPM.

9. Set MODE: CAL +90.

10. Adjust SIGNAL AMP: +90 to get peak-to-peak amplitude as in 2 above.

11. Adjust RATIO 90 to 150 : +90 to get a reading of +90 on DPM.

e. Field Use of Localizer Glide-Slope Monitor.

1. Connect monitor to +12 volt supply or battery.

2. Turn power on and allow monitor to warm up for 15 minutes.

3. Connect a localizer or glide-slope antenna to the proper input.

4. If desired, connect a chart recorder to REC-OUT jack on back of the chassis.

5. Set MODE: CAL-0, S1: LOC, S2: 1.

6. Adjust recorder pen position to get desired zero point on recorder.

7. Set MODE: CAL -90.

8. Adjust recorder gain to get desired -90 position.

9. Set MODE: CAL +90.

10. Check for proper +90 position on recorder.

11. Set MODE: NAV 11 for use with localizer signal, or MODE: UGR-2 for use with glide-slope signal.

12. Note that the range of the DPM is ±199.9. To read higher values set S2: 2.5. In this setting, the received SMQ (CDI) = 2.5x DPM reading.

13. For localizer use, select desired channel with NAV 11 frequency selector.

14. For glide-slope use, select the desired channel by setting the G S CHANNELING switches located on the top of the monitor box in accordance with the key located on the side of the UGR-2 receiver.

f. Maintenance.

1. Figure A-9 illustrates the general interrelationship of the various sections of the SMQ.

2. Figure A-10 illustrates the wiring of the mode switch.

3. Figures A-11 and A-12 illustrate the component layout on the 90/150 converter board and the calibrator board respectively.

4. Figure A-13 is the schematic of the SMQ power supply.

g. Parts List 90/150 Converter

Resistors

*R1 - 100K	* R17 - 3.3K	R33 - 10K
*R2 - 200K	R18 - 10K	R34 - 10K
*R3 - 200K	R19 - 10K	R35 - 10K
R4 - 10K	* R20 - 3.3K	R36 - 10K
R5 - 10K	* R21 - 47K	R37 - 10K
R6 - 680K	R22 - 10K	R38 - 10K
*R7 - 10.2K	R23 - 10K	R39 - 10K
R8 - 1K	R24 - 10K	R40 - 10K
R9 - 100K	R25 - 10K	* R41 - 3.3K
R10 - 100K	R26 - 10K	R42 - 15K
R11 - 2.2K	R27 - 10K	R43 - 10K
R12 - 10K	* R28 - 3.3K	R44 - 10K
R13 - 1.5K	R29 - 10K	R45 - 10K
R14 - 10K	R30 - 10K	R46 - 10K
R15 - 10K	* R31 - 47K	R47 - 10K
R16 - 10K	* R32 - 3.3K	

Capacitors

C1 - 10μf, 15v	C3 - 10μf, 30v	C5 - 10μf, 15v
C2 - .22μf, 25v	C4 - 10μf, 30v	C6 - 1000μf, 3v

Diodes

D1 - IN914	D3 - IN914
D2 - IN914	D4 - IN914

Pots

#1 - 10K	#3 - 10K	#5 - 10K
#2 - 10K	#4 - 10K	#6 - 10K

Op Amps

IC1A - SN747	IC3A - SN747	IC5A - SN747
IC1B - SN747	IC3B - SN747	IC5B - SN747
IC2A - SN747	IC4A - SN747	
IC2B - SN747	IC4B - SN747	

Miscellaneous

Filters	DC DC Inverters	Controls
90 Hz	1	GS Phase 1 Meg.
150 Hz	2	LOC Phase 1 Meg.
		ZERO, 5K
Divide Module	Regulated 5V Supply	GAIN, 5K
D210		
		Switches
Display		S1
2003		S2

h. Parts List Transfer Standard Calibrator

Resistors

R1 - 430	R10 - 1K	R19 - 10K
R2 - 30	R11 - 1K	*R20 - 56K
R3 - 10K	R12 - 10K	R21 - 47K
R4 - 10K	R13 - 100K	R22 - 68K
R5 - 1K	R14 - 100K	*R23 - 51K
R6 - 1K	R15 - 10K	R24 - 75K
R7 - 2K	R16 - 10K	R25 - 47K
R8 - 47K	R17 - 100K	
R9 - 4.7K	R18 - 100K	

Capacitors

C1 - 3-22pf	C3 - .05μf, 30v	C5 - .05μf, 30v
C2 - .01μf, 35v	C4 - .05μf, 30v	C6 - .05μf, 30v

Diodes

D1 - 914	D3 - 914
D2 - 914	D4 - 914

Pots

#1 - 10K	#3 - 10K	#5 - 2K
#2 - 10K	#4 - 2K	#6 - 2K

Op Amps

IC1 - 741	IC4A - $\frac{1}{2}$74107	IC6A - $\frac{1}{2}$74107
IC2A - $\frac{1}{2}$74107	IC4B - $\frac{1}{2}$74107	IC6B - $\frac{1}{2}$74107
IC2B - $\frac{1}{2}$74107	IC5A - $\frac{1}{2}$74107	
IC3 - 7490	IC5B - $\frac{1}{2}$74107	

Transistors

Q1 - 2N4401	Q3 - 2N4401	Q5 - 2N4403
Q2 - 2N4403	Q4 - 2N4401	

All resistors are $\frac{1}{4}$ watt except as noted by * and these are $\frac{1}{2}$ watt.

All potentiometers and controls are $\frac{1}{4}$ watt.

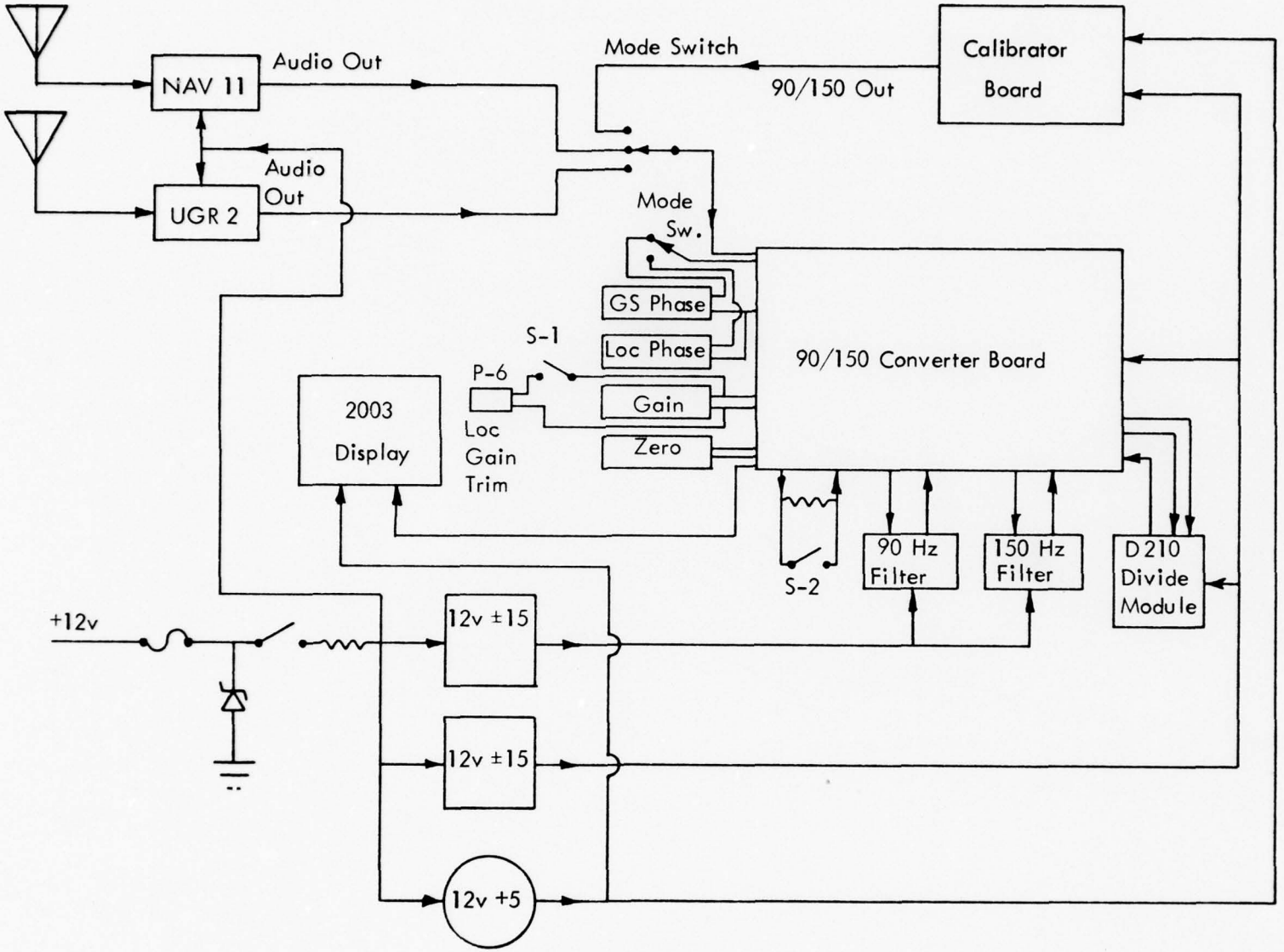

Figure A-9. Interconnect Diagram.

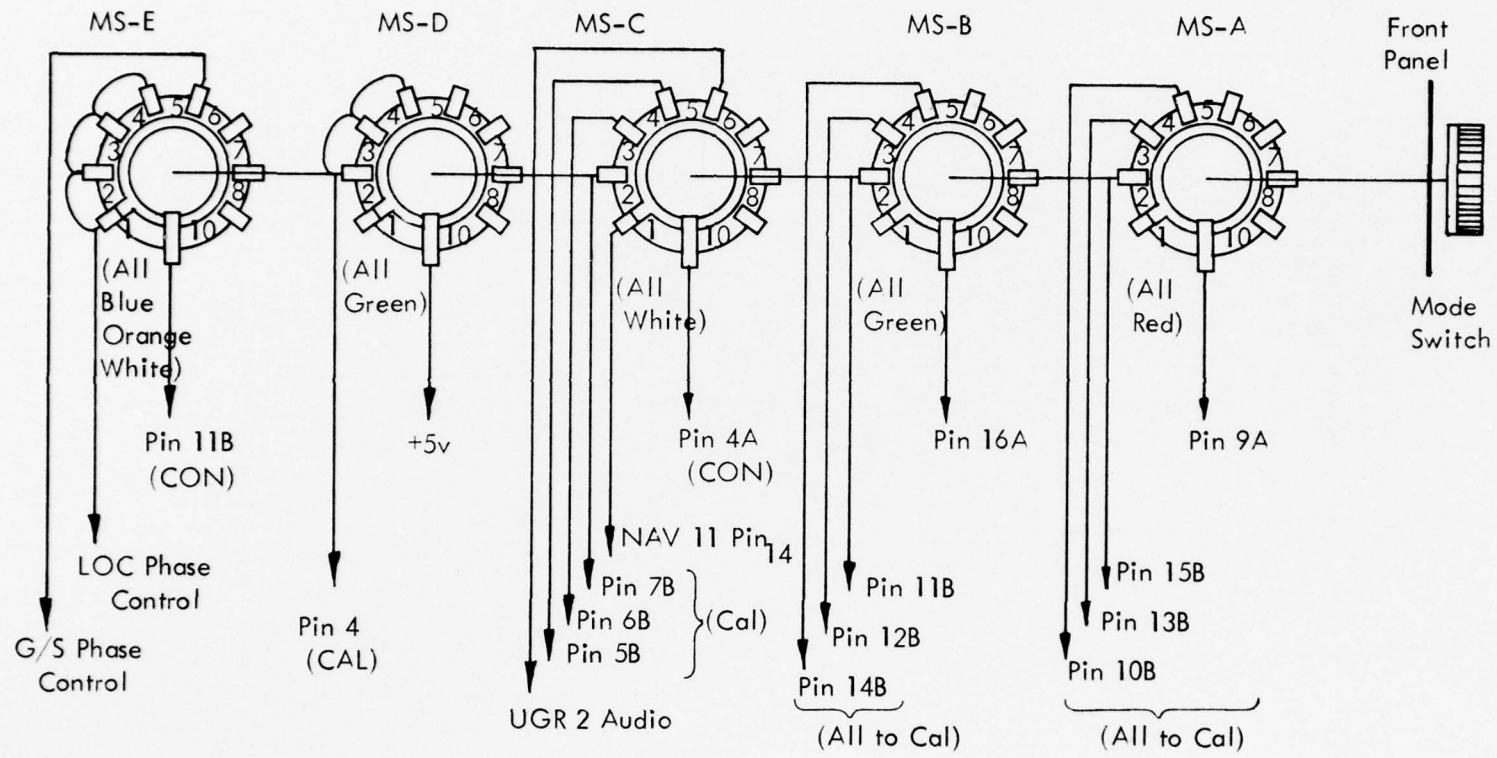

CON = 90/150 Converter Board
CAL = Calibrator Board

Figure A-10. Mode Switch.

*R4 AND R5 ARE UNDER IC1.
**R11 AND R12 ARE UNDER IC2.

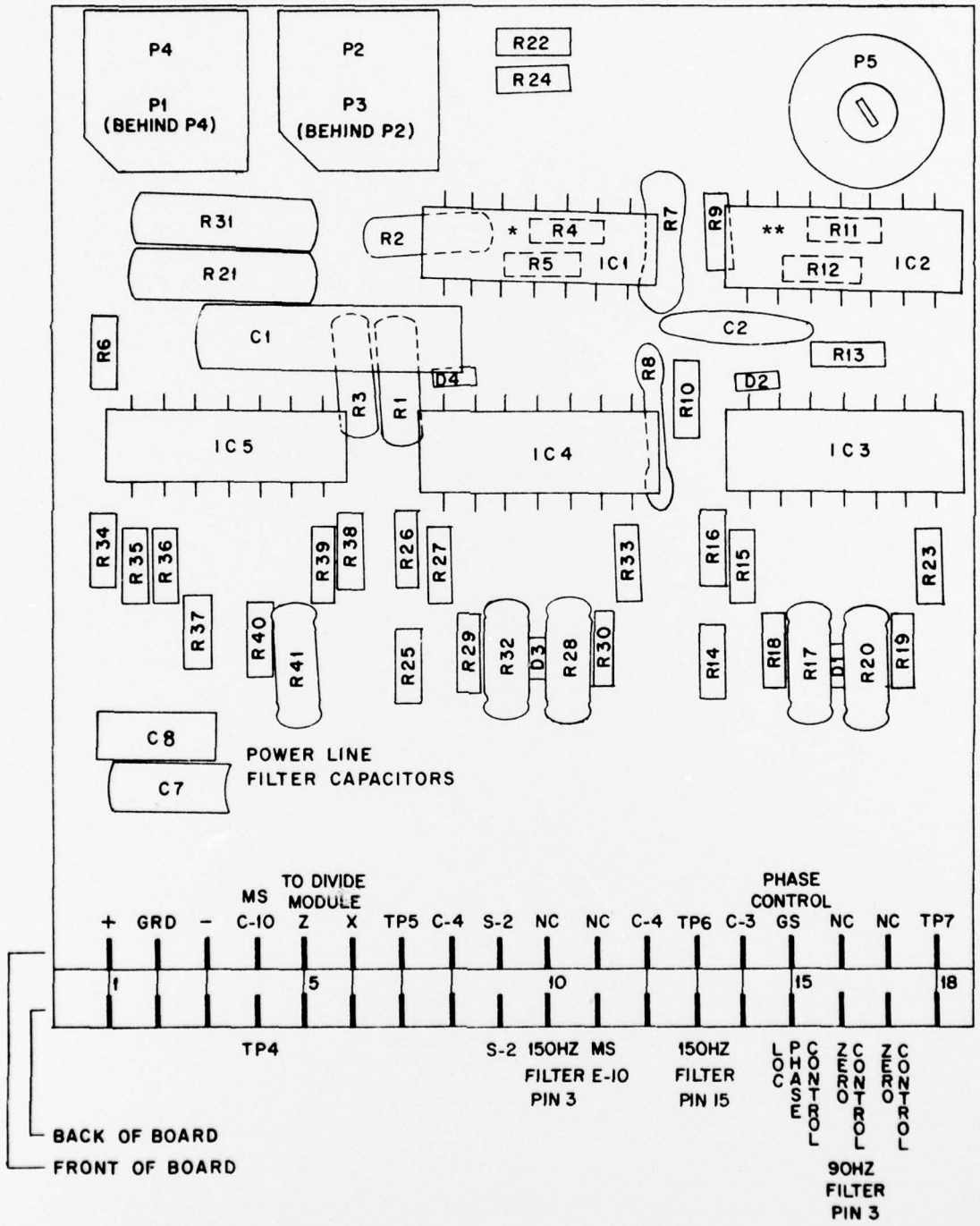

Figure A-11. 90/150 Converter Board.

*R1, R2, R7 ARE UNDER IC1.
**R2 = 30Ω IS MADE UP OF TWO 15Ω RESISTORS, ONE UNDER IC1 AND THE OTHER ON THE BACK OF THE BOARD.
***R24 ON BACK OF BOARD.
****C7 - POWER LINE BYPASS CAP.

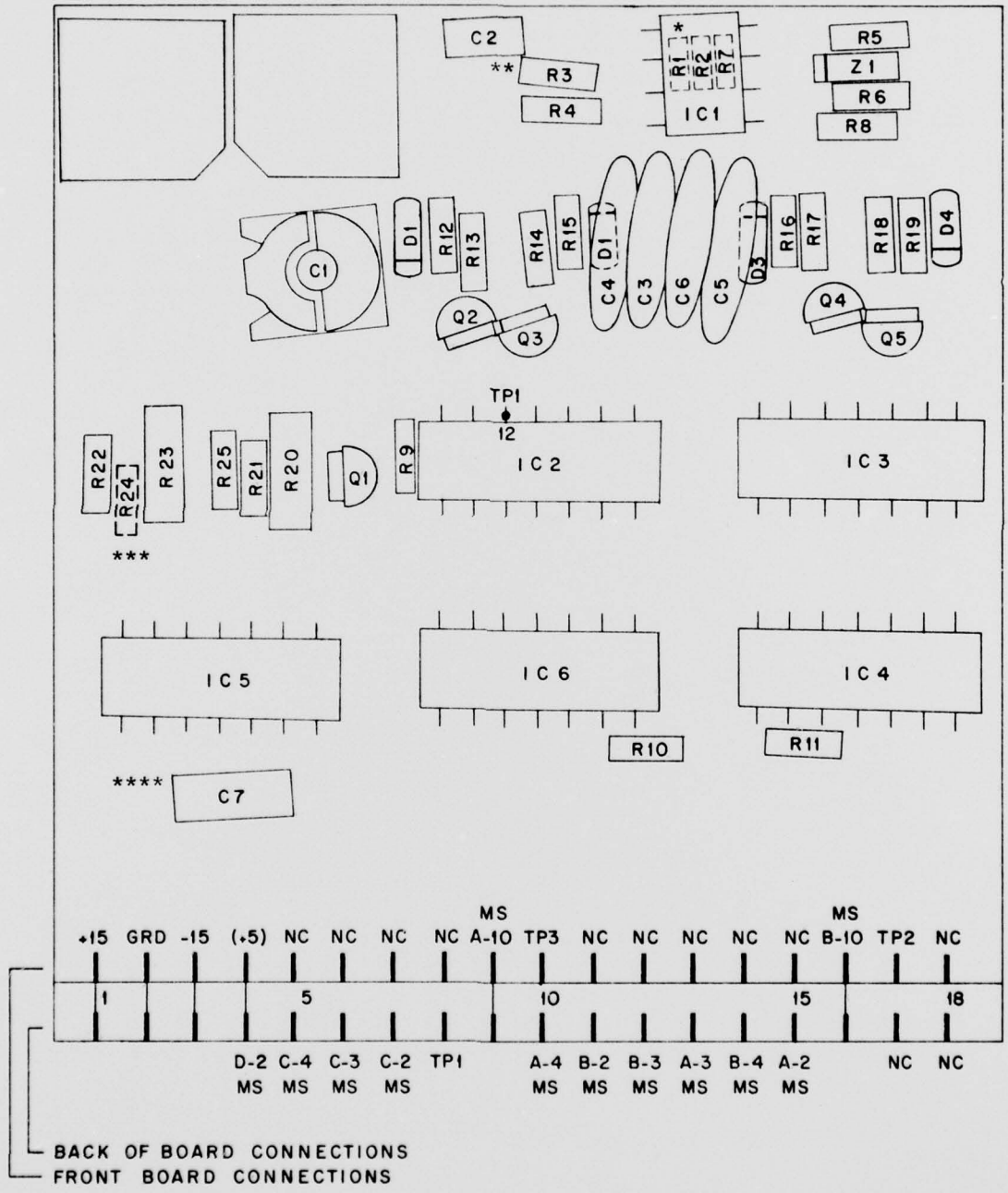

Figure A-12. Calibrator Board.

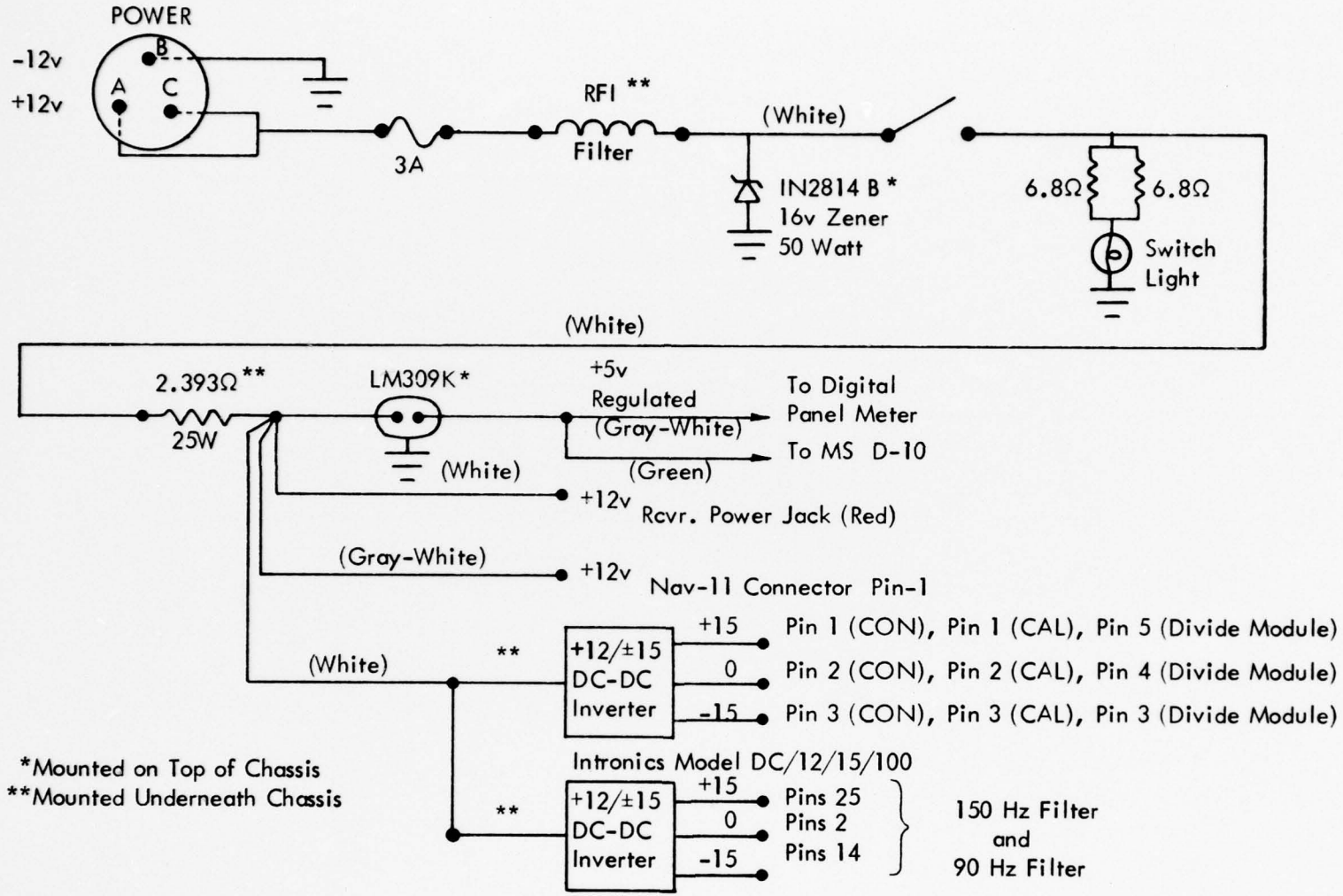

Figure A-13. Power Supply.

APPENDIX B. EXTRAPOLATION ALGORITHMS

1. DEVELOPMENT OF COMPUTER MODELS FOR THE FAR-FIELD GLIDE-SLOPE MONITOR

a. Computer Model for Predictor Algorithm. For the null reference system, with a height ratio fo 2:1 for sideband antenna to carrier antenna, the DDM is given by

$$DDM(\alpha) = K_1 \cos(K_2 \sin \alpha) \tag{1}$$

where
K_1 = 4mA
K_2 = carrier antenna height
α = elevation angle.

Due to the nonlinearity of the DDM equation, a general solution for K_1 and K_2 as a function of GCM probe angles and CDI measurements is not trivial.

In the technical report (Gradient Clearance Monitor Final Report, Contract DOT-FA69WA-2066 - Mod 7, October, 1972) the quasilinearization method was employed for the solution of the above problem. For reference, the method is briefly described here.

Let $t = \sin \alpha$

Then equation (1) becomes

$$DDM(t) = K_1 \cos(K_2 t) \tag{2}$$

satisfying the variational (differential) equation

$$\ddot{x}(t) + K_2^2 x(t) = 0 \tag{3}$$

where

$$x(t) = DDM(t)$$

by defining state variables

$$x_1 = x = DDM$$

$$x_2 = \dot{x} = \frac{d}{dt}(DDM)$$

$$x_3 = K_2^2$$

Equation (3) can be written in the state equation form

$$\begin{aligned} \dot{x}_1 &= x_2 = f_1 \\ \dot{x}_2 &= x_3 x_1 = f_2 \\ \dot{x}_3 &= 0 = f_3 \end{aligned} \tag{4}$$

with $x_1(0) = K_1$ and $x_2(0) = 0$ and $x_3(0) = K_2^2$.

In vector notation, equation (4) can be written as

$$\dot{\hat{x}} = \hat{f}(\hat{x}) \tag{5}$$

The boundary conditions b (ti) required for solution are measured microamperes of CDI at two known GCM probe elevations. Mathematically it means

$$[1\ 0\ 0] \begin{bmatrix} x_1(ti) \\ x_2(ti) \\ x_3(ti) \end{bmatrix} = b(ti) \qquad i = 1,2. \tag{6}$$

To begin we make an initial guess of the approximate solution $\hat{x}_1(t)$; then (N + 1) th approximation is obtained from the N th through the relation

$$\dot{\hat{x}}^{N+1} = \hat{f}(\hat{x}^N) + [\bar{J}_{\hat{x}^N} \hat{f}(\hat{x}^N)] [\hat{x}^{N+1}(t) - \hat{x}^N(t)] \tag{7}*$$

$$N = 0,1,2....$$

with boundary conditions given by

$$[1\ 0\ 0] \begin{bmatrix} x_1^{N+1}(ti) \\ x_2^{N+1}(ti) \\ x_3^{N+1}(ti) \end{bmatrix} = b(ti) \qquad i = 1,2 \tag{8}$$

---

*$\wedge$ indicates a vector and $-$ indicates a matrix.

The i j th element of the Jacobian matrix $[\bar{J}_{\hat{x}^N} \hat{f}(\hat{x}^N)]$

$$= \frac{\delta f_i(\hat{x})}{\delta x_j} \qquad \hat{x} = \hat{x}^N(t) \quad . \tag{9}$$

The general solution of equation (7) is

$$\hat{x}^{N+1}(t) = \bar{\Phi}(t)^{N+1} \hat{x}^{N+1}(0) + \hat{P}^{N+1}(t) \tag{10}$$

where $\bar{\Phi}(t)$ is the fundamental solution matrix of

$$\frac{\delta \bar{\Phi}^{N+1}(t)}{\delta t} = [\bar{J}_{\hat{x}^N} \hat{f}]\, \bar{\Phi}^{N+1}(t) \tag{11}$$

$$\bar{\Phi}^{N+1}(0) = \bar{I} = \text{identify matrix.}$$

and $\hat{P}(t)$, the particular solution vector, obeys the differential equation

$$\dot{\hat{P}}^{N+1}(t) = [\bar{J}_{\hat{x}^N} \hat{f}]\, \hat{P}^{N+1}(t) + \hat{f}(\hat{x}^N) - [\bar{J}_{\hat{x}^N} \hat{f}]\, \hat{x}^N \tag{12}$$

$$\hat{P}^{N+1}(0) = \hat{0}$$

The initial condition vector $\begin{bmatrix} x_1^{N+1}(0) \\ x_2^{N+1}(0) \\ x_3^{N+1}(0) \end{bmatrix}$ is determined from the boundary condition

$$[1\ 0\ 0] \begin{bmatrix} \Phi_{11}^{N+1}(ti)\, x_1^{N+1}(0) + \Phi_{12}^{N+1}(ti)\, x_2^{N+1}(0) + \Phi_{13}^{N+1}(ti)\, x_3^{N+1}(0) + P_1^{N+1}(ti) \\ \Phi_{21}^{N+1}(ti)\, x_1^{N+1}(0) + \Phi_{22}^{N+1}(ti)\, x_2^{N+1}(0) + \Phi_{23}^{N+1}(ti)\, x_3^{N+1}(0) + P_2^{N+1}(ti) \\ \Phi_{31}^{N+1}(ti)\, x_1^{N+1}(0) + \Phi_{32}^{N+1}(ti)\, x_2^{N+1}(0) + \Phi_{33}^{N+1}(ti)\, x_3^{N+1}(0) + P_3^{N+1}(ti) \end{bmatrix}$$

$$= b(ti) \qquad i = 1,2 \,. \tag{13}$$

which from (14) is

$$J\left[\hat{x}^{N+1}(0),\ \hat{q}_D\right] = \left\| \hat{q}_D - \hat{\gamma}^{N+1} - \bar{\psi}\,\hat{x}^{N+1}(0) \right\|^2_{\bar{R}^{N+1}}$$

with respect to $\hat{x}^{N+1}(0)$. In these equations, $\bar{R}^{N+1}$ is a non-negative-definite, symmetric matrix indicating the relative importance of each measurement. The estimate of the initial condition vector is determined if the gradient of J with respect to $\hat{x}^{N+1}(0)$ is equated to zero and solved for $\hat{x}^{N+1}(0)$. The result is:

$$\hat{x}^{N+1}(0) = \left[\bar{\psi}^T \bar{R}^{N+1} \bar{\psi}\right]^{-1} \bar{\psi}^T \bar{R}^{N+1} \left[\hat{q}_D - \hat{\gamma}^{N+1}\right].$$

This problem was programmed for solution on the Ohio University IBM Model 360-44 computer, and the predicted values for on-path and width CDI were thus obtained.

c. Use of a Priori Knowledge of On-Path Value of CDI. The controlled fault experiments performed at the Ohio University test site in Michigan were of such a nature that the theoretical value of on-path CDI should remain at zero while the path width would broaden. Use was made of this fact by altering the formulation for determining the initial-value vector from the predictive algorithm. The initial-value vector is found from:

$$\hat{x}^{N+1}(0) = \left[\bar{\psi}^T \bar{R}^{N+1} \bar{\psi}\right]^{-1} \bar{\psi}^T \bar{R}^{N+1} \left[\hat{q}_D - \hat{\gamma}^{N+1}\right]$$

where $\bar{R}^{N+1}$ is a non-negative definite, symmetric matrix whose diagonal elements specify the relative weights given to elements of the $\hat{q}_D$ vector.

The problem was retormulated to accommodate an additional data point in the q_D vector of probe measurement values. The sixth value in this vector was given a value of zero to correspond with the expected CDI value at the 3-degree elevation angle value. All diagonal elements of $\bar{R}^{N+1}$ were given values of one with the exception of $R^{N+1}(6,6)$ which was given a fractional value to lessen the effect of the a priori on-path CDI value on the resultant predicted values. It was found, that a value for $R^{N+1}(6,6)$ of 0.05 would significantly improve the correspondence between the predicted values of on-path and width CDI and the values measured at the far-field television tower probes. The problem inherent with the

weighted on-path value occurs when the on-path value may change with changing environmental conditions. In such a case, the weighted zero value for on-path CDI tends to hold this value lower than the realized value.

d. Conversion of Algorithm to Double-Precision Arithmetic. Since the prediction algorithm used for the FFGSM is iterative in nature, and experience has shown that even very small errors in such algorithms can produce significant error after several iterations, the predictor algorithm was converted so that all computations were executed in double-precision arithmetic. The results obtained by using the double-precision arithmetic were identical with those obtained with single-precision version. This computer program, therefore, should be used for computation because of its faster execution time and smaller core storage requirements.

2. EFFECTS OF IMPERFECTLY REFLECTING GROUND PLANE ON MODEL PREDICTIONS

In using the equation DDM (α) = $K_1 \cos (K_2 \sin \alpha)$ in deriving the differential equations describing DDM versus elevation angle, it is assumed that the reflection surface for the glide-slope electromagnetic radiation field has an ideal reflection coefficient. At a given installation this assumption may not be valid due to differing types of soil, ground cover, moisture content, etc.

At the Ohio University Experimental Snow Site in Ravenna Township, Michigan, a sampling probe was used to determine the CDI values at different elevation angles at the far-field glide-slope monitor antenna in order to construct the actual curve of DDM versus elevation angle. The curve constructed from this data is shown in Figure B-1 along with the curve given by the theoretical model. It can be seen from the figure that the values of CDI detected by the monitor antennas will be somewhat less than the corresponding values given by the model equation.

In order to predict the width angle and on-path values of CDI accurately from the model equations, a nominal field which produced a CDI of 150 microamperes at the width angle and zero microamperes at the on-path angle at the television tower in the far field, was transmitted and the corresponding values of CDI were measured at the FFGSM probes. A correction factor was then determined which, when multiplied by the measured CDI value at a given elevation angle, would give the theoretical CDI value for that angle. Correction factors were determined for each of the five angles at which sampling antenna probes were positioned on the antenna mast. The raw data obtained during the extensive fault tests of February 14 and April 3-4 were multiplied by the correction factors before the quasilinearization algorithm was used on the digital computer to predict width and path CDI values.

The method used for the predictions gave good results for amplitude faults and for phase faults up to $\pm$ 30 degrees. For phase faults in excess of 30 degrees the predictions were not accurate enough to reliably indicate the path structure. Further work was initiated for the purpose of improving these predictions, either by implementing a different model formulation, or by improving upon the present model.

Once $x_1^{N+1}(0)$, $x_2^{N+1}(0)$ and $x_3^{N+1}(0)$ are found, then unknowns $K_1 = x_1^{N+1}(0)$ and $K_2^2 = x_3^{N+1}(0)$ are determined. With these constants known, DDM can be readily determined at the clearance angle. (A similar formulation can be made for the problem with no specific height ratio for sideband antenna to carrier antenna. For details, please refer to Gradient Clearance Monitor, October, 1972 report.)

In the above method two measurements need not uniquely determine the exact solution. To alleviate the uniqueness difficulties, and also difficulties which arise from noisy measurements and poor modeling, an additional number of measurements, hence boundary conditions, are added.

b. Linear Regression Technique Added to Model. According to Sage[1] it is sometimes expedient in the presence of measurement noise, to provide a number of measurements in excess of the number required for a unique solution, and to apply a regression analysis on these measurements in order to "smooth" the data. In accordance with this theory, three probes in excess of the two required were added to the FFGSM receiving antenna array; and a linear regression technique was used to provide a realistic estimate of the true solution. For noisy data, linear regression provides an unbiased estimate for solution, and for noise-free data, linear regression solves the problems posed by uniqueness difficulties.

In order to employ linear regression, the following formulation is defined:

Let $\hat{q}_D$ be the five-dimensional set of measured points corresponding to the five probe elevation angles b(ti). Let $\hat{q}^{N+1}$ be the corresponding set of points obtained from $\hat{x}^{N+1}(t)$.

Then:

$$\hat{q}^{N+1} = \bar{\psi}\hat{x}^{N+1}(0) + \hat{\gamma}^{N+1} \qquad (14)$$

where the matrix $\bar{\psi}$ and the vector $\hat{\gamma}$ are composed of elements from the fundamental solution matrix $\bar{\Phi}(t)$ and the particular solution vector $\hat{P}(t)$ evaluated at the appropriate elevation angles. An estimate of the initial-condition vector is to be determined which minimizes the differences between $\hat{q}_D$ and $\hat{q}^{N+1}$ in a least-squares sense.

Mathematically, minimize:

$$J\left|\hat{x}^{N+1}(0), \hat{q}_D\right| = \left\| \hat{q}_D - \hat{q}^{N+1} \right\|^2_{\bar{R}^{N+1}}$$

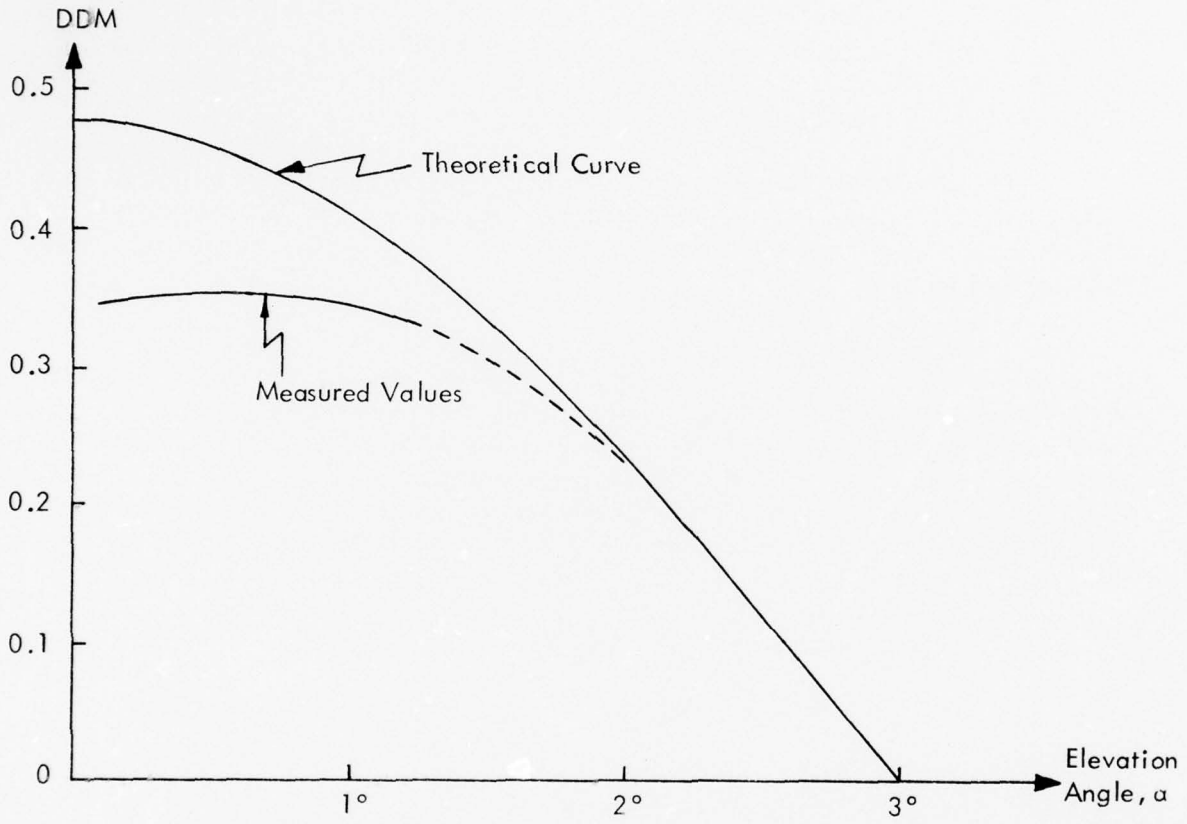

Figure B-1. Measured and Theoretical Values of DDM versus Elevation Angle.

3. CUBIC EQUATION MODEL FOR DDM versus ELEVATION ANGLE CURVE

In an attempt to develop a mathematical model which would provide more accurate predictions of width angle and on-path CDI, a cubic equation was used whose form is $K_1\alpha^3 + K_2\alpha^2 + K_3\alpha + K_4 = \text{DDM}$. The curve represented by this equation can be made to match closely the DDM versus elevation angle curve over the range of interest as shown in Figure B-2 if the values of K_1, K_2, K_3, and K_4 are chosen properly. The determination of the proper K values is the job of the quasilinearization algorithm in the computer modeling procedure. The set of differential equations representing this cubic formulation were programmed into the algorithm and run on the computer with the data collected at the Michigan Snow Site. The results showed that there was no significant improvement in the predictions over the previously described model. Therefore, it was reasoned that regardless of the formulation for the DDM versus elevation angle curve, the difficulty encountered in trying to accurately predict on-path and width values is a result of using values on the curve in a low gradient region to specify boundary conditions. Variations of small magnitude in such a region will result in large variations in the prediction of values on the steep portion of the curve.

4. INVESTIGATION OF EFFECTS OF RANDOM PERTURBATIONS

In order to analyze the computer model of the far-field glide-slope monitor for sensitivity to noisy measurements at the sampling probes, two methods were used to perturb the experimental values of CDI obtained from the April 3 Michigan Snow Site data.

The first method used uniformly random numbers whose magnitude ranged from zero to two. The signs of the numbers were also chosen randomly. Thus, the perturbations of the experimental data varied from -2 microamperes to +2 microamperes. These random values were added to the experimental data points to simulate random noise in the measuring system. The results of the computer analysis showed that the predicted values of width CDI varied in magnitude by as much as 9 microamperes, while the predicted path CDI varied in magnitude by as much as 14 microamperes.

The second method used a pseudo-random number generator with a Gaussian distribution with zero mean and a standard deviation of 0.4. The maximum magnitude of the random changes introduced by this method was 3.2 microamperes. The computer analysis showed that the predicted width CDI had a maximum variation in magnitude of 14 microamperes and the predicted path CDI had a maximum variation of 22 microamperes.

The foregoing perturbation analysis indicates that for measurement noise whose magnitudes are no greater than two or three microamperes, we may expect prediction variations of as much as 14 microamperes in width CDI predictions, and 22 microamperes in path CDI predictions. The magnification of the measurement variations in the CDI predictions are believed to be a result of attempting to predict the values on a trajectory in a high gradient region by setting the boundary conditions on a region of the trajectory

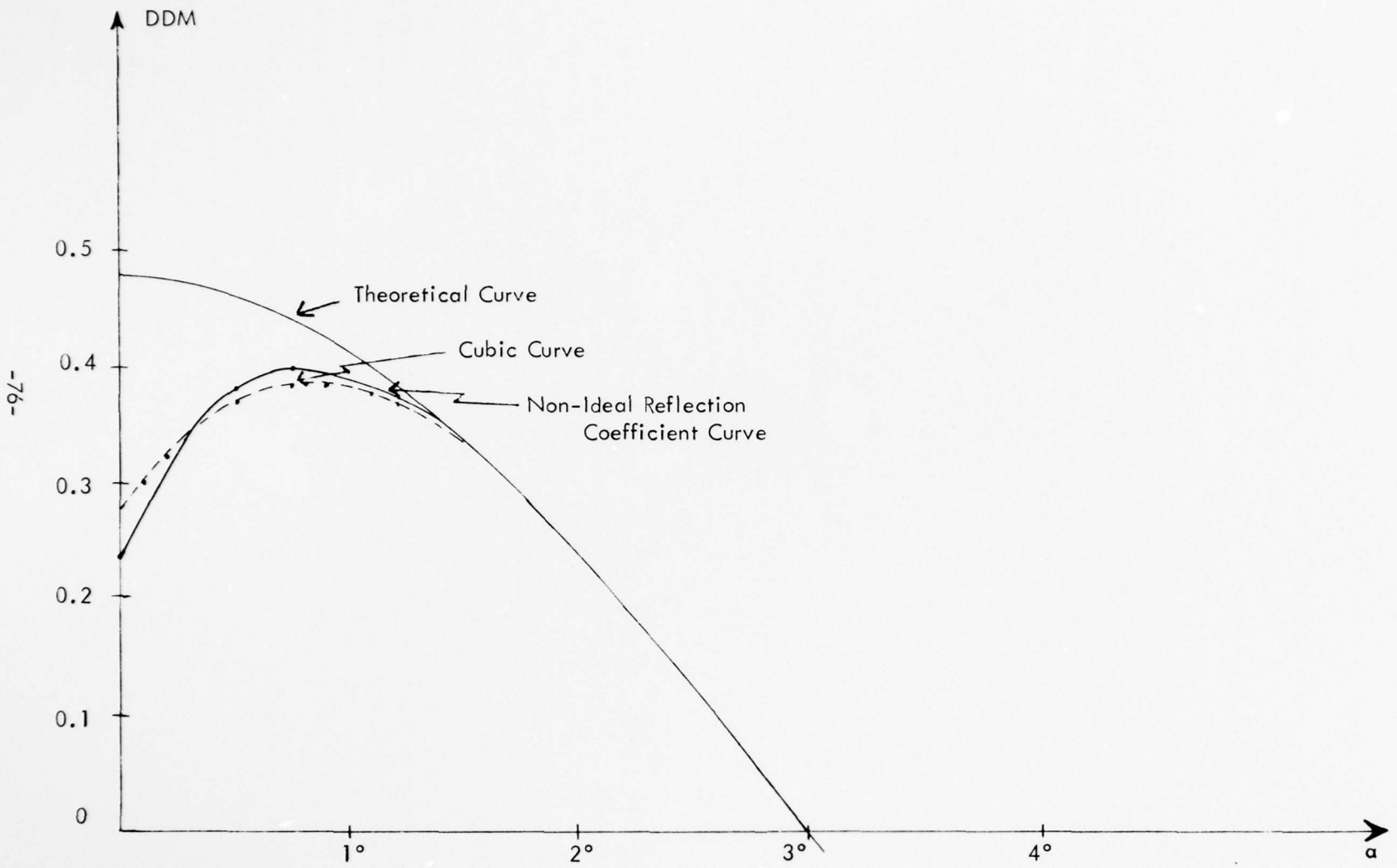

Figure B-2. Comparison of Theoretical Perfect Reflection, Theoretical Non-Ideal Reflection, and Cubic Curve of DDM versus Elevation Angle.

where the gradient is low. The low gradient of the measurable portion of the CDI versus elevation angle curve is due in large part to a ground surface whose reflection coefficient is less than perfect. This results in a flattening of the curve at elevation angles of 1.25 degrees or less. The necessity of using boundary point measurements in the low gradient region of the curve is due to the obstruction height constraint.

5. PROXIMITY PHASE ERROR AT FAR-FIELD GLIDE-SLOPE MONITOR

To determine the possible effect of phase differences in the signal received by different antennas of the receiving array, the proximity phase error was calculated for the top and bottom antennas of the array. The equation for determining proximity phase error is given by

$$B_p = -\left|\frac{H^2 - h^2}{2S}\right| \frac{360}{\lambda}$$

where

B_p = proximity phase error, in degrees

H = height of sideband antenna, in feet

h = height of carrier antenna, in feet

S = distance from base of transmitting antenna to receiving antenna, in feet

and λ = wavelength of signal, in feet.

The geometry of the antennas is shown in Figure B-3. The proximity phase error with respect to the top antenna is -7.91°; with respect to the bottom antenna, -8.52°. The difference in phase between the signal received by the top antenna and that received by the bottom antenna is $-7.91° - (-8.52°) = 0.61°$. For the two signals to be exactly in phase, the upper antenna would need to be moved 0.06 inch nearer the transmitting array. Thus, the effect of proximity phase error across the receiving antenna array is considered to be insignificant.

6. REFERENCES

[1] Sage, A. P., Optimum Systems Control, Prentice-Hall, Inc., Englewood Cliffs, N. J., 1968, p. 442.

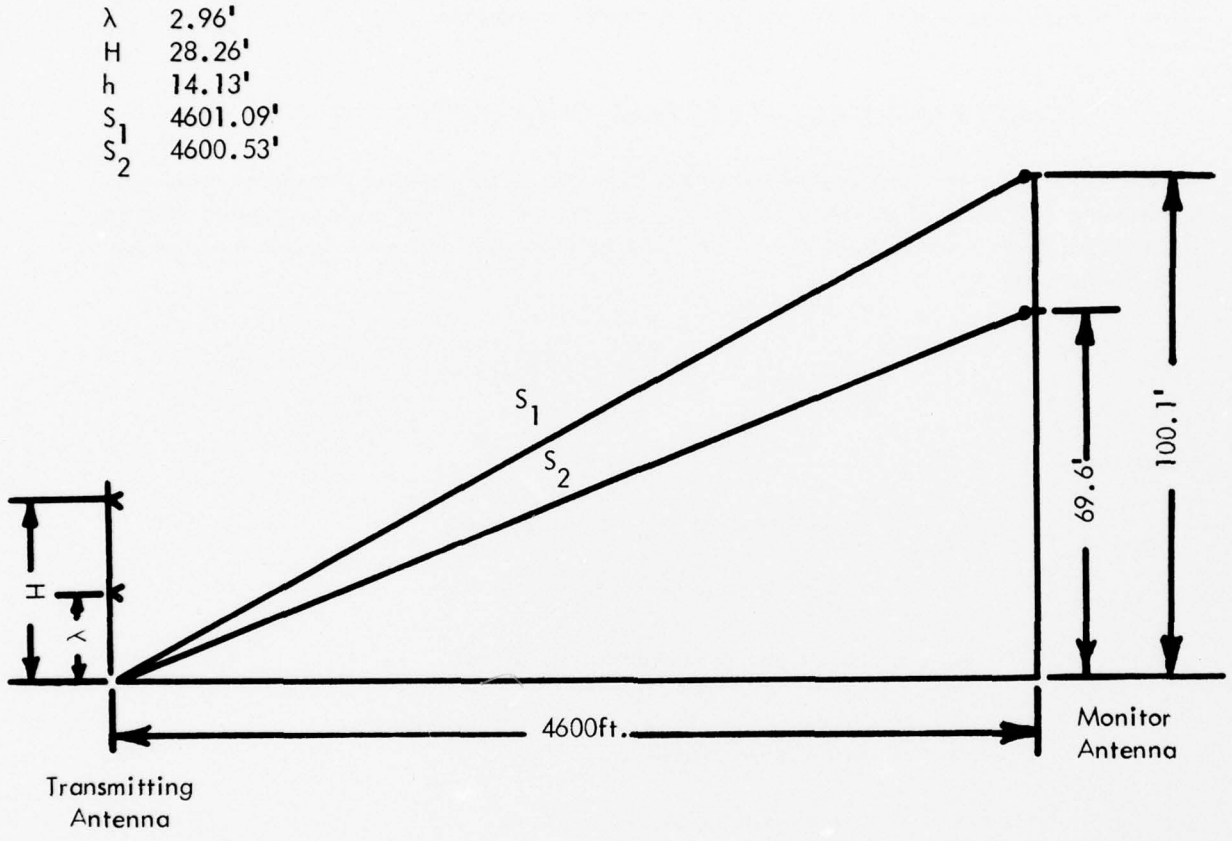

Figure B-3. Geometry of Proximity Phase Error Model.